Defense Threat Reduction Agency
8725 John J. Kingman Road, MS
6201 Fort Belvoir, VA 22060-6201

DTRA-TR-10-70

TECHNICAL REPORT

Composite-Nanoparticles Thermal History Sensors

Approved for public release; distribution is unlimited.

June 2012

HDTRA1-07-1-0015

Gang Chen

Prepared by:
Mechanical Engineering Dept.
77 Massachusetts Ave., 3-260
Cambridge, MA 02139.

DESTRUCTION NOTICE:

Destroy this report when it is no longer needed.
Do not return to sender.

PLEASE NOTIFY THE DEFENSE THREAT REDUCTION AGENCY, ATTN: DTRIAC OP-ONIU, 8725 JOHN J. KINGMAN ROAD, MS-6201, FT BELVOIR, VA 22060-6201, IF YOUR ADDRESS IS INCORRECT, IF YOU WISH THAT IT BE DELETED FROM THE DISTRIBUTION LIST, OR IF THE ADDRESSEE IS NO LONGER EMPLOYED BY YOUR ORGANIZATION.

CONVERSION TABLE

Conversion Factors for U.S. Customary to metric (SI) units of measurement.

MULTIPLY → BY → TO GET

TO GET ← BY ← DIVIDE

angstrom	1.000 000 x E -10	meters (m)
atmosphere (normal)	1.013 25 x E +2	kilo pascal (kPa)
bar	1.000 000 x E +2	kilo pascal (kPa)
barn	1.000 000 x E -28	meter^2 (m^2)
British thermal unit (thermochemical)	1.054 350 x E +3	joule (J)
calorie (thermochemical)	4.184 000	joule (J)
cal (thermochemical/cm^2)	4.184 000 x E -2	mega joule/m^2 (MJ/m^2)
curie	3.700 000 x E +1	*giga bacquerel (GBq)
degree (angle)	1.745 329 x E -2	radian (rad)
degree Fahrenheit	$t_k = (t°f + 459.67)/1.8$	degree kelvin (K)
electron volt	1.602 19 x E -19	joule (J)
erg	1.000 000 x E -7	joule (J)
erg/second	1.000 000 x E -7	watt (W)
foot	3.048 000 x E -1	meter (m)
foot-pound-force	1.355 818	joule (J)
gallon (U.S. liquid)	3.785 412 x E -3	meter^3 (m^3)
inch	2.540 000 x E -2	meter (m)
jerk	1.000 000 x E +9	joule (J)
joule/kilogram (J/kg) radiation dose absorbed	1.000 000	Gray (Gy)
kilotons	4.183	terajoules
kip (1000 lbf)	4.448 222 x E +3	newton (N)
kip/inch^2 (ksi)	6.894 757 x E +3	kilo pascal (kPa)
ktap	1.000 000 x E +2	newton-second/m^2 ($N-s/m^2$)
micron	1.000 000 x E -6	meter (m)
mil	2.540 000 x E -5	meter (m)
mile (international)	1.609 344 x E +3	meter (m)
ounce	2.834 952 x E -2	kilogram (kg)
pound-force (lbs avoirdupois)	4.448 222	newton (N)
pound-force inch	1.129 848 x E -1	newton-meter (N-m)
pound-force/inch	1.751 268 x E +2	newton/meter (N/m)
pound-force/foot^2	4.788 026 x E -2	kilo pascal (kPa)
pound-force/inch^2 (psi)	6.894 757	kilo pascal (kPa)
pound-mass (lbm avoirdupois)	4.535 924 x E -1	kilogram (kg)
pound-mass-foot^2 (moment of inertia)	4.214 011 x E -2	kilogram-meter^2 ($kg-m^2$)
pound-mass/foot^3	1.601 846 x E +1	kilogram-meter^3 (kg/m^3)
rad (radiation absorbed dose)	1.000 000 x E -2	**Gray (Gy)
roentgen	2.579 760 x E -4	coulomb/kilogram (C/kg)
shake	1.000 000 x E -8	second (s)
slug	1.459 390 x E +1	kilogram (kg)
torr (mm Hg, 0^0 C)	1.333 22 x E -1	kilo pascal (kPa)

*The Becquerel (Bq) is the SI unit of radioactivity; 1 Bq = 1 event/s.

**The Gray (Gy) is the SI unit of absorbed dose.

REPORT DOCUMENTATION PAGE

Form Approved
OMB No. 0704-0188

PLEASE DO NOT RETURN YOUR FORM TO THE ABOVE ORGANIZATION.

1. REPORT DATE *(DD-MM-YYYY)*	2. REPORT TYPE	3. DATES COVERED *(From - To)*
16/09/2010	Final Technical Report	1 Jul 2007 / 30 Jun 2010

4. TITLE AND SUBTITLE
Compoisite-Nanoparticles Thermal History Sensors

5a. CONTRACT NUMBER

5b. GRANT NUMBER
HDTRA1-07-1-0015

5c. PROGRAM ELEMENT NUMBER

6. AUTHOR(S)
Chen, Gang

5d. PROJECT NUMBER

5e. TASK NUMBER

5f. WORK UNIT NUMBER

7. PERFORMING ORGANIZATION NAME(S) AND ADDRESS(ES)
Mechanical Engineering Department
77 Massachusettes Ave 3-260
Cambridge, Ma 02139

8. PERFORMING ORGANIZATION REPORT NUMBER

9. SPONSORING/MONITORING AGENCY NAME(S) AND ADDRESS(ES)
DTRA-R&D Enterprise
8725 John J. Kingman Rd
Ft. Belvoir, VA 22060

10. SPONSOR/MONITOR'S ACRONYM(S)
DTRA

11. SPONSOR/MONITOR'S REPORT NUMBER(S)

12. DISTRIBUTION/AVAILABILITY STATEMENT
Approved for public release; distribution is unlimited.

13. SUPPLEMENTARY NOTES
N/A

14. ABSTRACT

15. SUBJECT TERMS

16. SECURITY CLASSIFICATION OF:			17. LIMITATION OF ABSTRACT	18. NUMBER OF PAGES	19a. NAME OF RESPONSIBLE PERSON
a. REPORT	b. ABSTRACT	c. THIS PAGE			Gang Chen
Unclassified	Unclassified	Unclassified	UU		19b. TELEPHONE NUMBER *(Include area code)* (617) 253-0006

Objectives:

This project aims at developing composite nanostructure-based (core-shell nanoparticles, heterostructure nanowires, and nano-flakes) temperature history sensors for recording the thermal environment that biological agent simulants experience during the testing of agent-defeat weapons. Such nanocomposite nanostructures transform the time-dependent temperature environment into the spatial mass-diffusion profile that can be interrogated after the experiment. The nanostructures are chosen so that they can be attached to bio-agent stimulant during the experiments without interfering with their functionality. Tasks include developing the composite nanostructure synthesis method, the mass-diffusion diagnosis method, analytical tools that map the mass-diffusion profile into temperature history.

Status of Effort:

During the time period of the project, thermal history dependences of the structure, size, shape, and melting point of several types of nanoparticles were studied by TEM. A variety of nano-sized particles with different shapes and quantum dots (QDs) were studied in broad temperature range from room temperature to over 900 °C. Photoluminescence (PL) of core/shell CdSe/ZnS QDs in different sizes were used as a tool to exam their interfacial mass diffusion processes due to the temperature change.

Hot-stage TEM studies show that all nanoparticles exhibit strong temperature dependence on their size. For example, the average size of Ag nanospheres is 4 nm at 300 °C while 14 nm at 700 °C. The PL of core/shell CdSe/ZnS QDs in size of ~ 5 nm show strong dependence on their temperature history. The PL could be detected after sample was heated up to 800 °C in a time frame of seconds. The quenching of PL intensity and blue-shift of the PL spectra with increasing temperature and heating time provides an optical route to read out the thermal history. Quantitative relationship between nanoparticles size and heating temperature has been established using TEM technique and PL technique. We showed that Ag nanoparticle size changes can be used to record temperature profile created by electron-beam heating and read out after the event, and that QDs are sensitive to ms heating..

Accomplishments:

We have achieved two major accomplishments. One is quantitative relationship between nanoparticle structural properties and heating temperature studied on TEM to investigate the thermal history of the nanoparticles, such as the temperature dependence of nanosphere diameter. Another is quantitative optical study to develop a relatively simple readout mechanism of the thermal history. Optical studies using photoluminescence techniques (PL) is to characterize nanoparticles and link their optical properties to their structure and structural changes. The characteristics of PL peak shift and intensity quench can be described by simple models that link to the thermal mass diffusion. The two characteristics can be used as two fingerprints in one dots sensor to record a single thermal exposure event with heating temperature and duration to be retrieved. With ~5 nm sized larger QDs, the sensitivity of heating time has been tested in tens of milliseconds with temperature up to about 500 °C.

1. TEM STUDIES

1.1. Syntheses of nanoparticles

We synthesized several types of nanoparticles using a Parr reactor for the project.

- **Silicon nanoparticles**

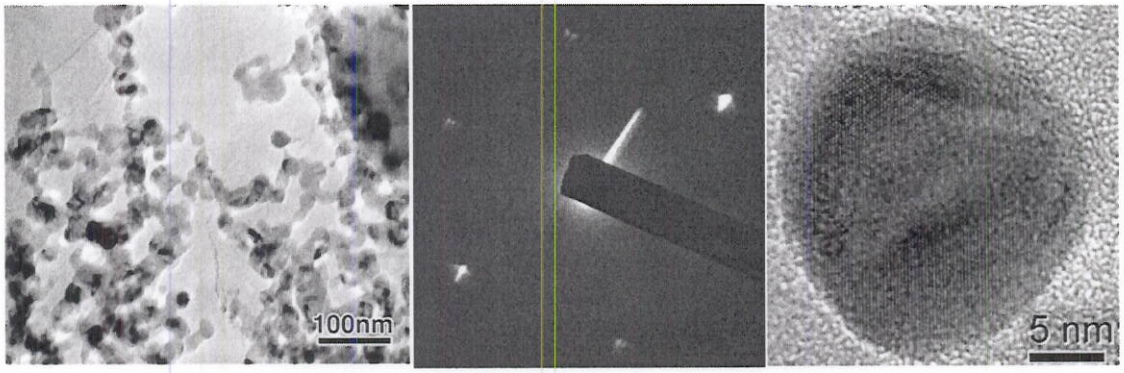

Figure 1.1-1. TEM images of synthesized Si nanoparticles. a) TEM image at low magnification, b) SAED of an individual nanoparticle, and c) HRTEM of a Si nanoparticle.

The silicon nanoparticles are synthesized using chemical method in solution. Figure 1.1-1 shows TEM images of the synthesized Si nanoparticles. The size of Si nanoparticles is in the range of 10-80 nm. SAED and HRTEM of individual nanoparticles indicate that the synthesized nanoparticles are single crystals.

- **PbTe nanocubes**

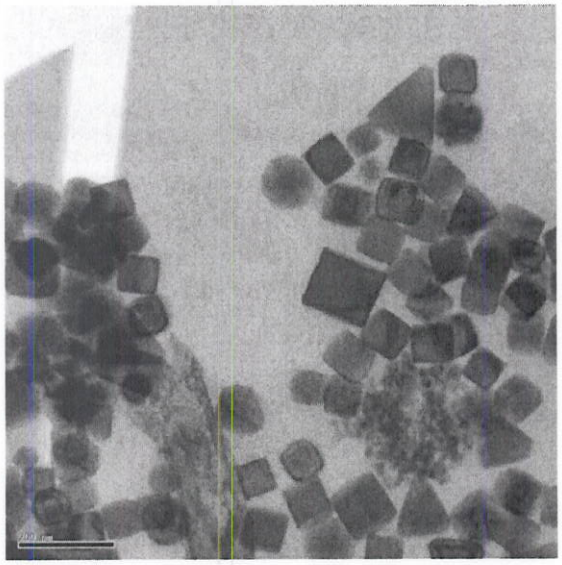

Figure 1.1-2. TEM image of PbTe nanocubes.

Figure 1.1-2 shows the TEM image of PbTe nanocubes synthesized. The prepared nanocubes have a uniform size of around50nm.

- **PbSe nanoflakes**

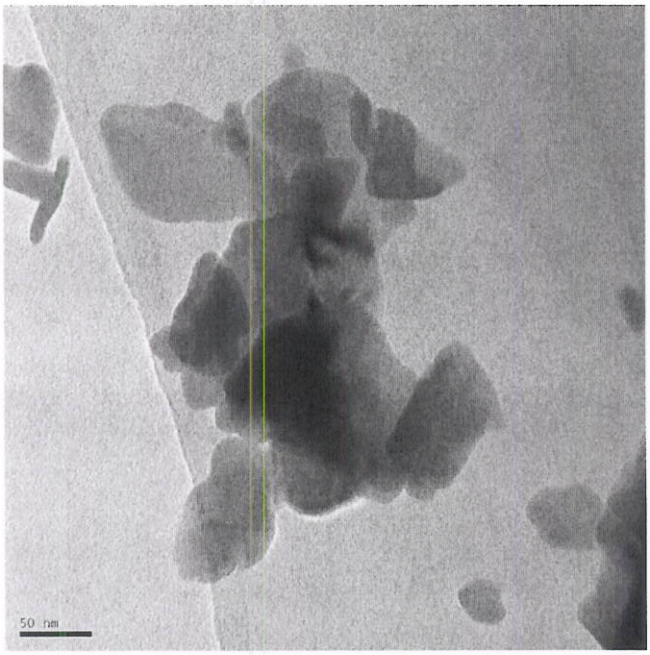

Figure 1.1-3. TEM image of PbSe nanoflakes.

TEM image in Figure 1.1-3 shows the PbSe nanoflakes are irregular. The size of PbSe nanoflakes is in nanometers.

1.2. TEM heating holder

To heat the nanoparticles, we designed a TEM heating holder. Figure 1.2-1 shows the heating holder and the controller. The nanoparticles are heated in air or in vacuum.

When the nanoparticles are heated in vacuum, the nanoparticles are deposited on TEM grids. Then the TEM grid is loaded in the heating holder. After the TEM holder is loaded into TEM column, the TEM grid is heated up and kept for a certain time in vacuum (1×10^{-5}Pa). The heating temperature can be reached to 1000 °C from room temperature in one minute and cooled down to room temperature in two minutes. The size and microstructure of the nanoparticles are examined at the heating temperature or examined at room temperature after the nanoparticles are cooled down.

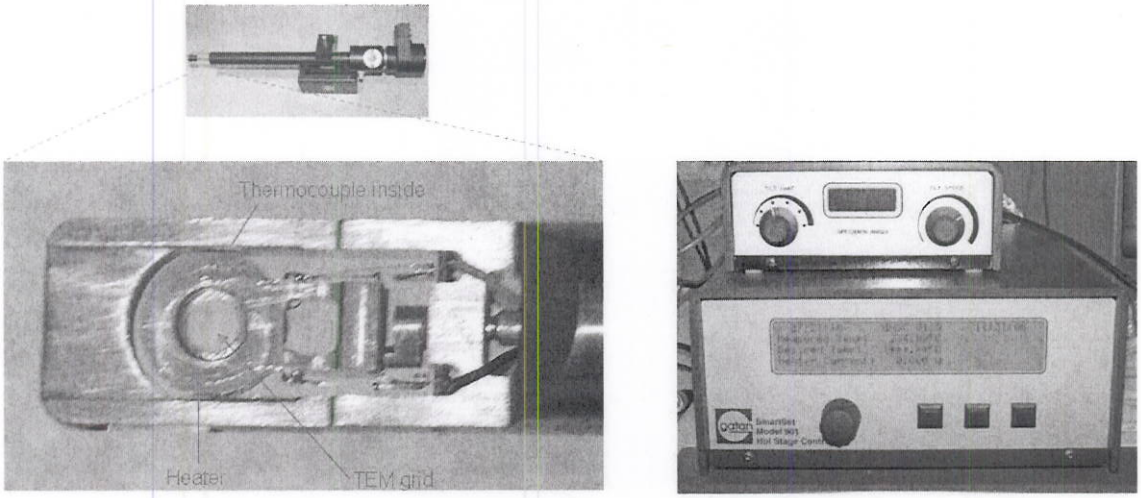

Figure 1.2-1. TEM heating holder and controller. Left: holder Right: controller.

When the nanoparticles are heated in air, the nanoparticles are deposited on TEM grids first. Then the TEM grid with nanoparticles is heated in a tube furnace in air. The heating temperature and heating time are controlled from several seconds to several minutes. After heating in air, the TEM grids are loaded to TEM heating holder. After the TEM holder is loaded into TEM column, the heated nanoparticles are examined at room temperature.

1.3. *Ex-situ* TEM observation of heated nanoparticles in air

We heat nanoparticles in air and then examine the nanoparticles on TEM at room temperature.

- **Heating of Si nanoparticles in air**

The silicon nanoparticles are heated in air for 5 minutes and *ex-situ* observed on TEM. Figure 1.3-1 shows the TEM images of same nanoparticles after being heated. After heated for 5 min at different temperatures (RT – 500 °C), the shape and size of Si nanoparticles are unchanged with a temperature heated up to 500 °C in air.

A group of PbSe nanoflakes are heated for one minute at temperature up to 500 °C in air. There is no big difference before and after heating.

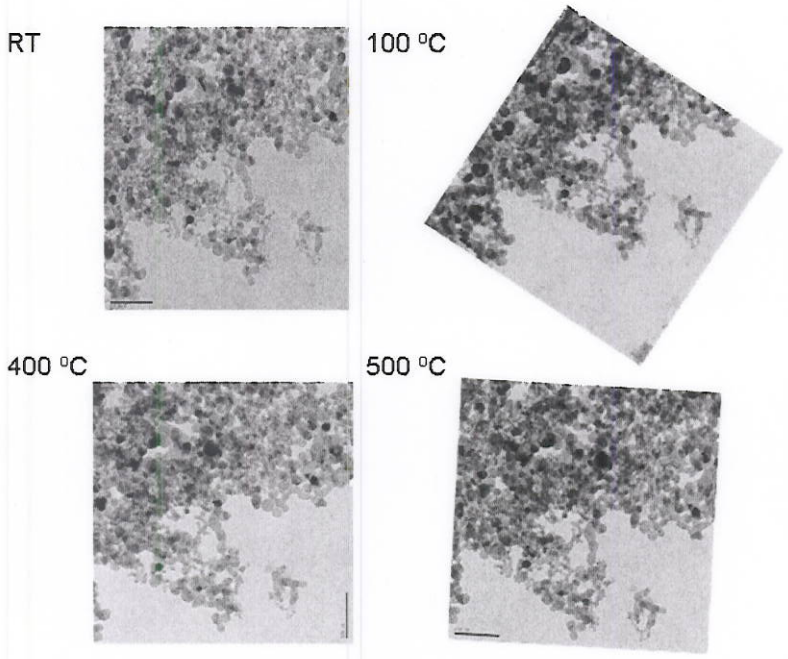

Figure 1.3-1. *Ex-situ* TEM images of Si nanoparticles after heated at different heating temperatures for 5 min in air.

- **Heating of PbSe nanoflakes in air**

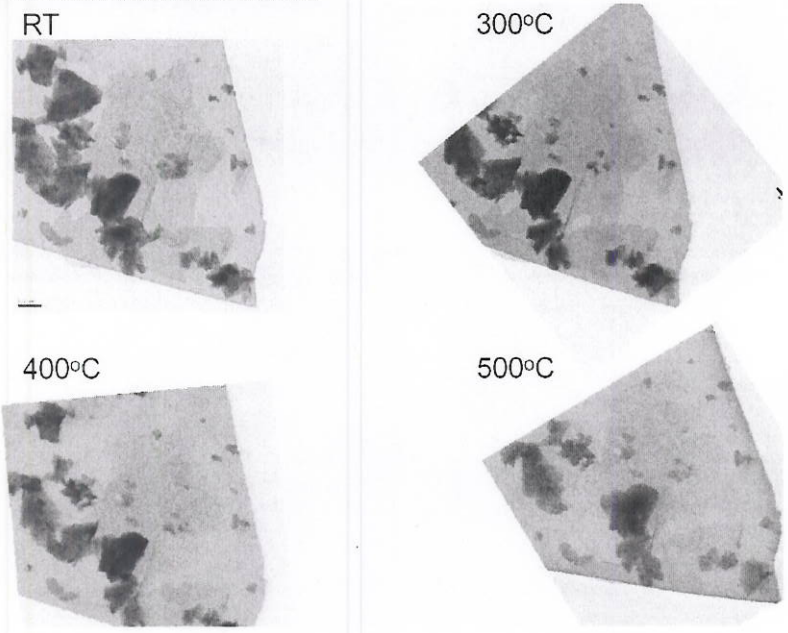

Figure 1.3-2. *Ex-situ* TEM images of PbSe nanoflakes heated at different heating temperatures for 1 min in air.

- **Heating of PbTe naotubes in air**

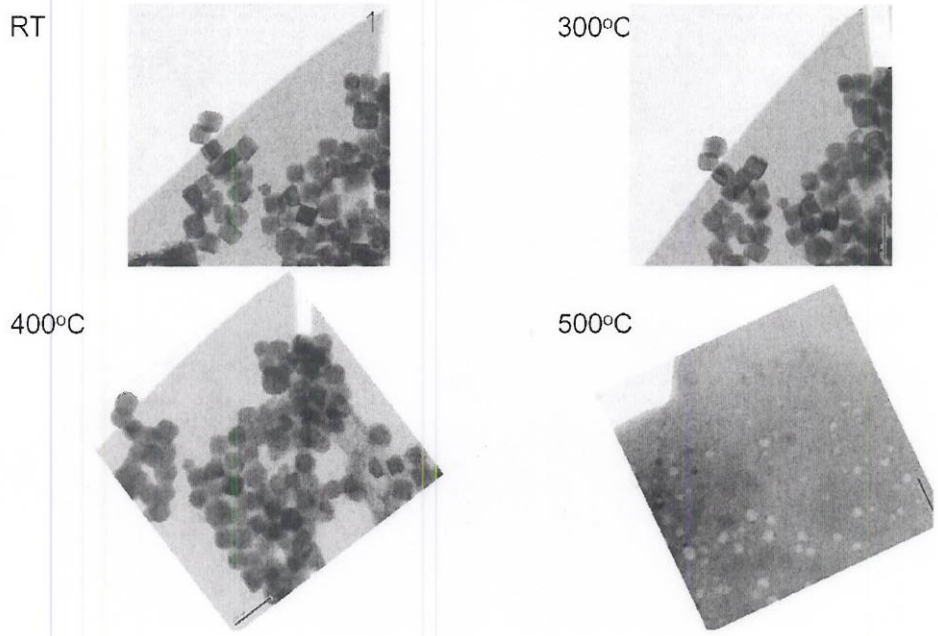

Figure 1.3-3. *Ex-situ* TEM images of PbTe nanocubes heated in air.

PbTe nanoparticles are heated in air at different temperatures to monitor their melting and size changes. The sample is heated in ambient with heating time of 10 seconds at each sample temperature (Figure 1.3-3). The corner of the nanocubes is rounded at 400 °C. The nanotubes disappear at 500 °C.

Ag nanoparticles are purchased. Figure 1.3-4 shows the size of the nanoparticles. HRTEM shows that the particles are single crystalline.

- **Heating of Ag nanoparticles in air**

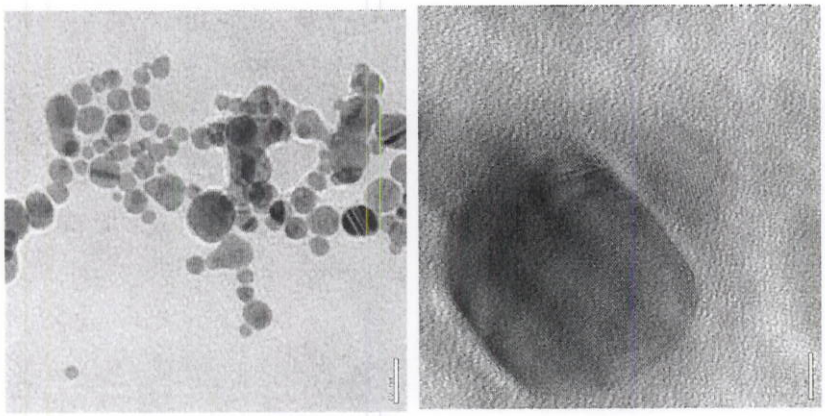

Figure 1.3-4. TEM of as-received Ag nanoparticles

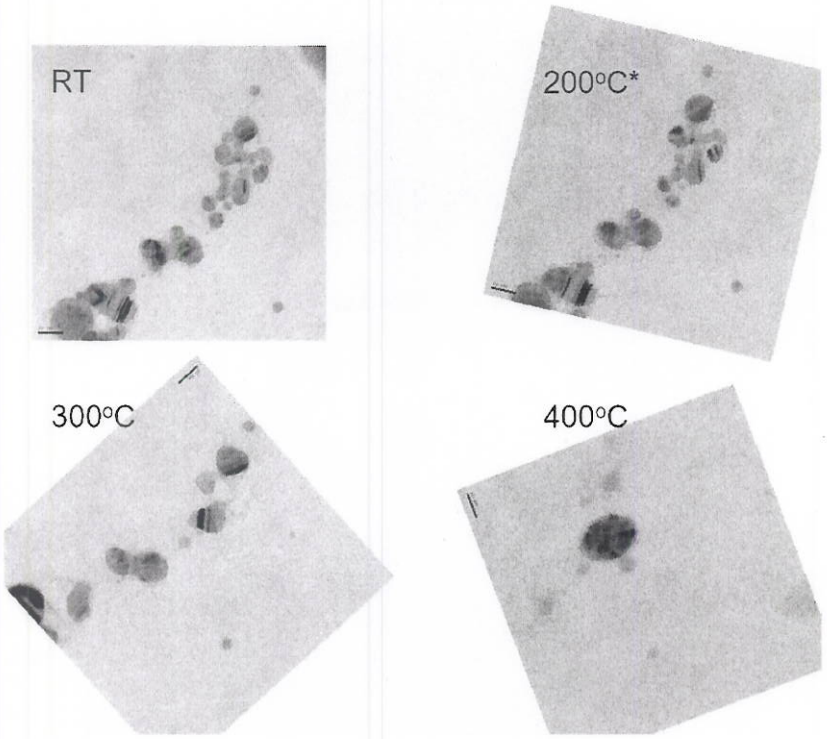

Figure 1.3-5. *Ex-situ* TEM images of Ag nanoparticles heating in air.

A group of Ag particles with distributed sizes are heated in ambient air for one minute at heating temperatures up to 400 °C. Figure 1.3-5 shows the TEM images of the nanoparticles. After heating in air, the smaller nanoparticles disappear while the bigger nanoparticles grow.

In addition to the heating temperature, the heating time also affects the size and morphology of the nanoparticles. Figure 1.3-6 shows a group of Ag nanoparticles heated in air at 400 °C with heating time from 2 seconds to 5 minutes respectively. The smaller nanoparticles evaporate with heating time and only bigger nanoparticles survive.

CdSe/ZnS core/shell quantum dots are purchased. Figure 1.3-7 shows the HRTEM images of the QDs. The size is about 5 nm and the QDs are good single crystals. The QDs are heated in air and then observed on TEM.

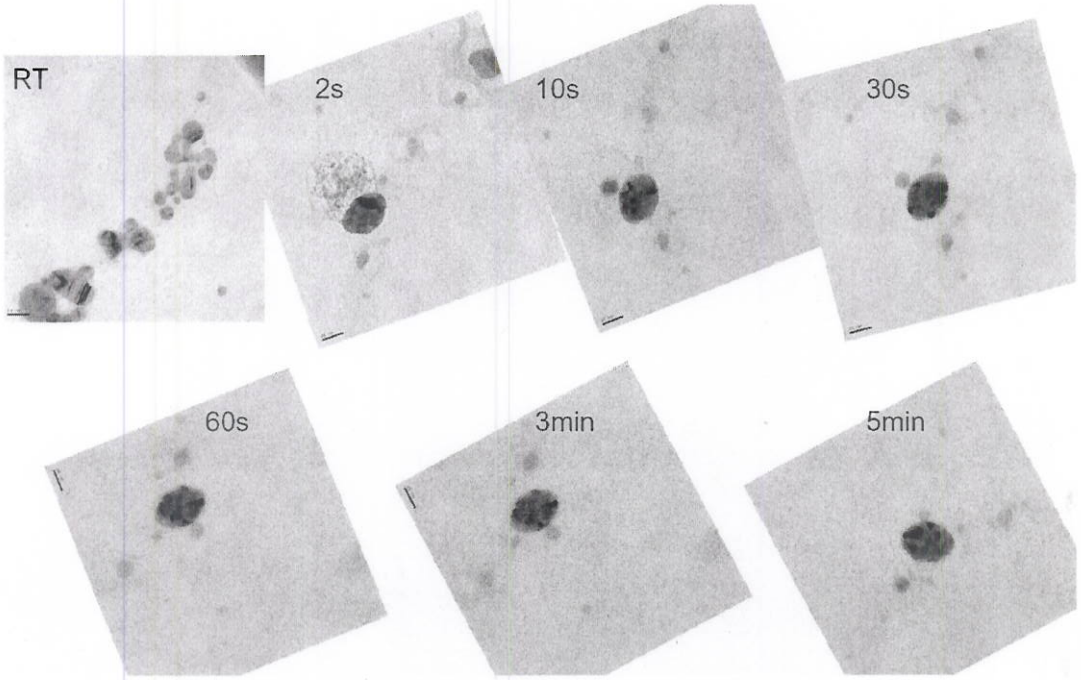

Figure 1.3-6. *Ex-situ* TEM images of Ag nanoparticles heated at 400 °C in air for different heating time.

- **Heating of CdSe QDs in air**

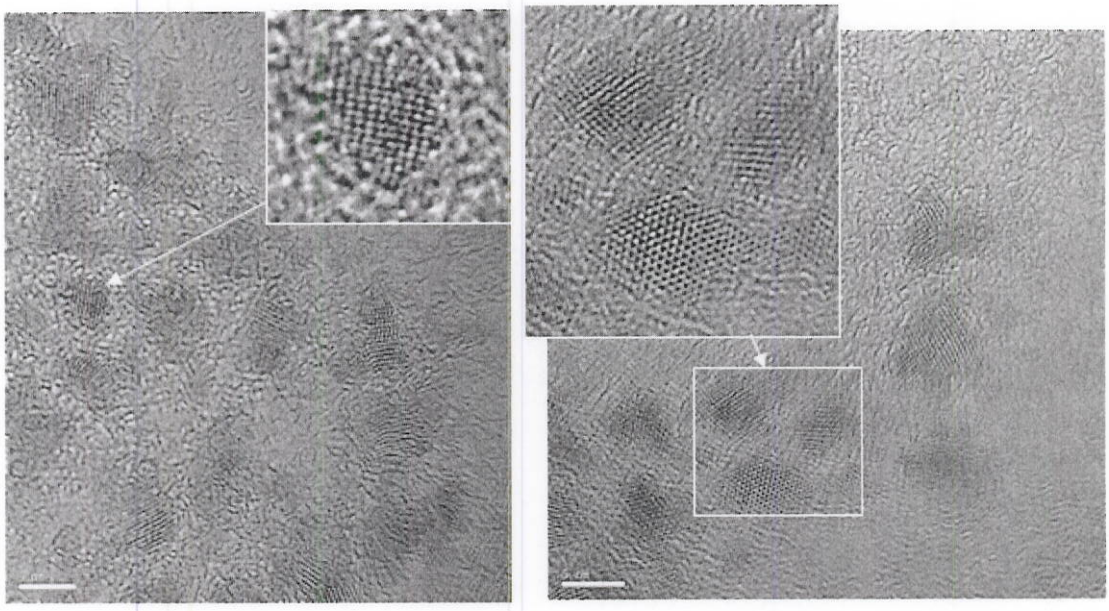

Figure 1.3-7. HRTEM images of CdSe/ZnS quantum dots.

Figure 1.3-8 shows the HRTEM images of heated quantum dots in air. QDs are heated up to 200 °C in air. The size of QDs decreases with heating temperature.

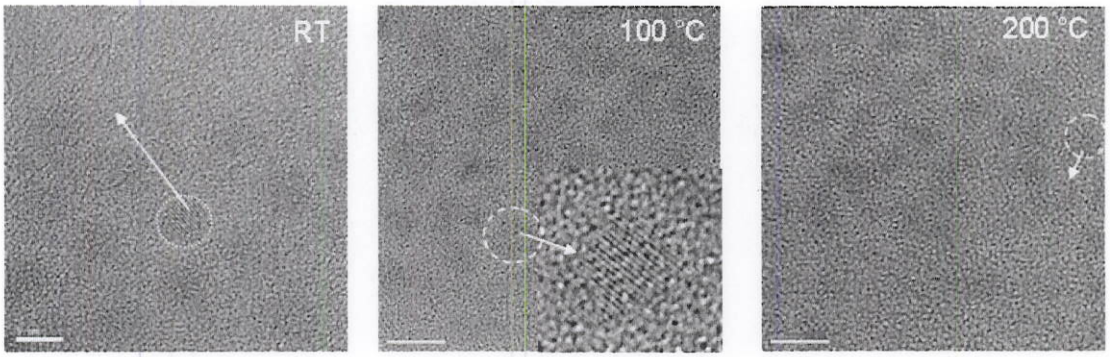

Figure 1.3-8. HRTEM images of CdSe QDs heated in air.

QDs are also heated at higher temperatures up to 450 °C. Because of the thermal stability of the supporting films, no QDs are observed. Figure 1.3-9 shows the morphology of TEM supporting films after heating in air. The supporting carbon film is broken at 400 °C in air and totally burned at 450 °C. A new kind of TEM grids are needed to resistant the oxidization.

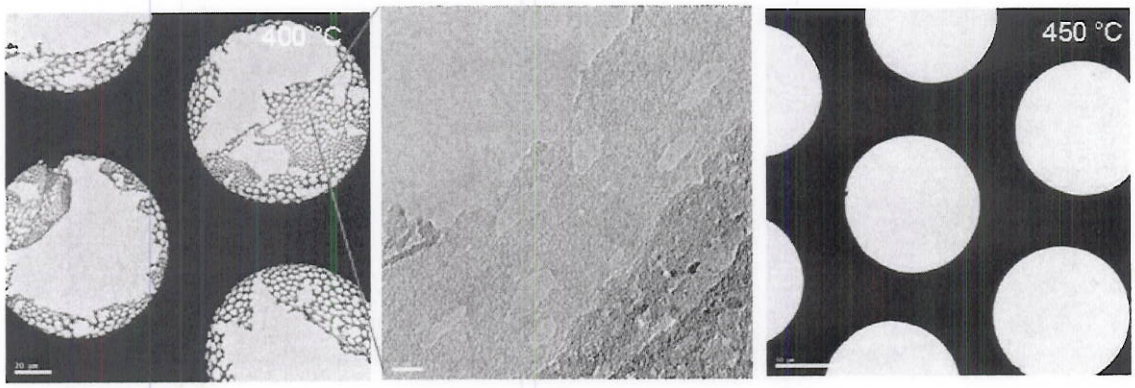

Figure 1.3-9. TEM images of QDs after heated at higher temperature.

1.4. *In-situ* heating of nanoparticles in vacuum

The nanoparticles are heated in vacuum and *in-situ* observed on TEM. Two methods are employed to examine the morphology and size of nanoparticles. The nanoparticles can be examined at high temperature or examine at room temperature after being heated.

Figure 1.4-1 shows a HRTEM image of silver nanoparticle heated at 500 °C. At the heating temperature, the surface of the nanosphere is melted while the solid core is still crystalline. SAED is consisted of halos and diffraction spots, indicating the nanosphere is consisted of solid phase and liquid phase.

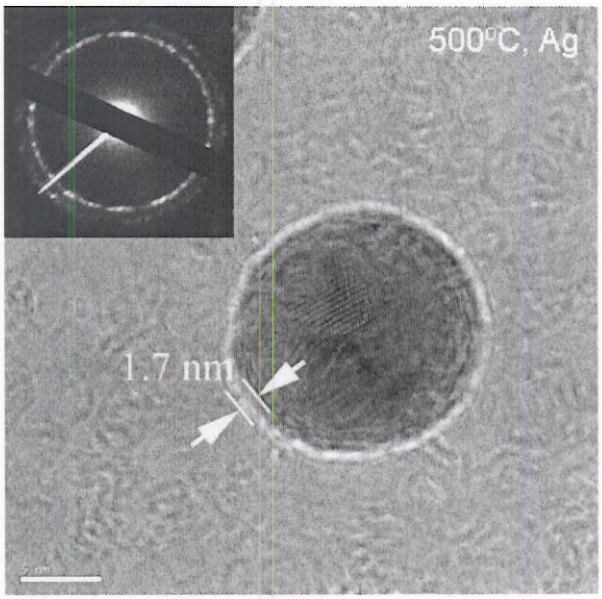

Figure 1.4-1. *In-situ* HRTEM image of Ag nanosphere taken at 500 °C in vacuum. Inset is SAED of the heated nanosphere.

Figure 1.4-2 shows more Ag nanoparticles heated in vacuum. When heated at high temperature, the smaller particles (marked by dashed lines) disappear while the bigger particles grow because smaller nanoparticles have higher vapor pressures. The higher vapor pressure causes the higher evaporation rate of smaller nanoparticles.

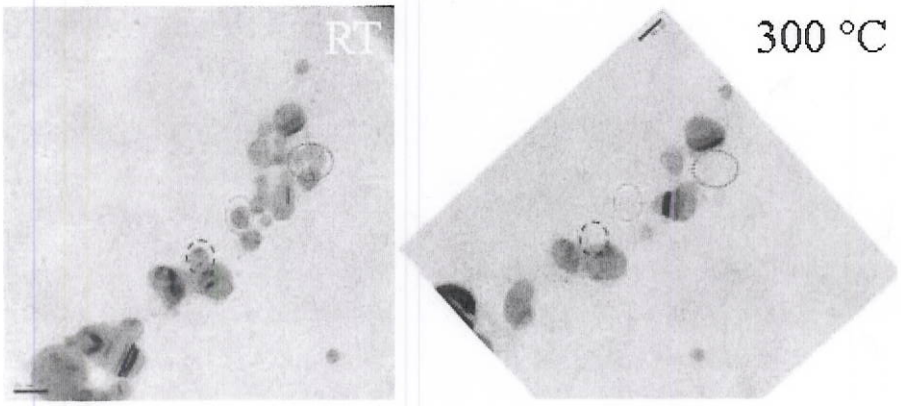

Figure 1.4-2. *In-situ* TEM images of Ag nanoparticles taken at heating temperature.

When the as-received Ag nanoparticles are heated in vacuum, much smaller Ag nanoparticles grow on the supporting film. Figure 1.4-3 shows TEM image of a silver cluster before and after heating. Before heating, only a silver cluster consisted of as-received silver nanoparticles are

deposited on the supporting film. After heating, many smaller nanoparticles grow besides the silver cluster. More experiments (inset in Figure 1.4-3) indicate the grown nanoparticles are uniform and cover the whole TEM grids. Then the grown Ag nanoparticles can be used for thermometer.

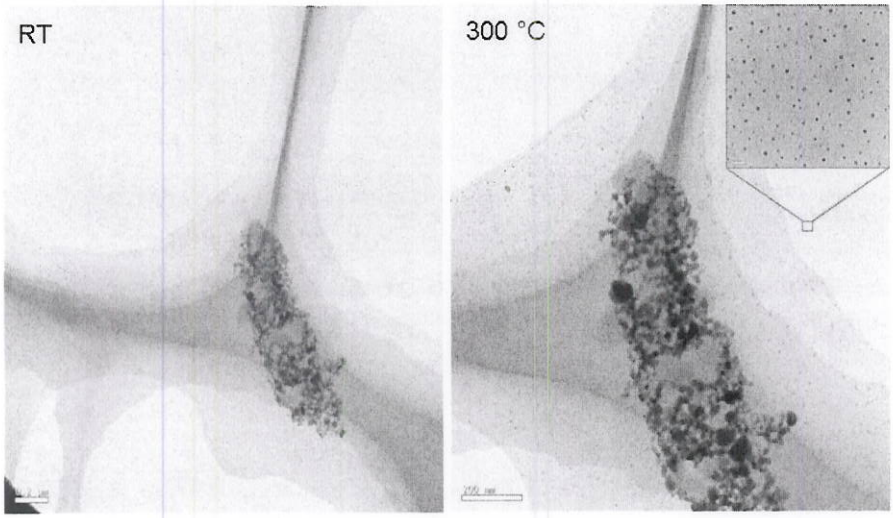

Figure 1.4-3. TEM of Ag particles. Left: no heated; right: heated.

The as-received silver nanoparticles are heated at different temperature in vacuum. Figure 1.4-4 shows TEM images of such produced nanoparticles. Each sample experiences only one certain heating temperature. The size of the grown Ag nanoparticles increases with the heating temperature.

After quickly cooled down to the room temperature, the size distribution of the grown silver nanoparticles is examined at room temperature. Statistical analysis indicates that the size distribution of Ag nanoparticles at heating temperature is almost same as that at room temperature.

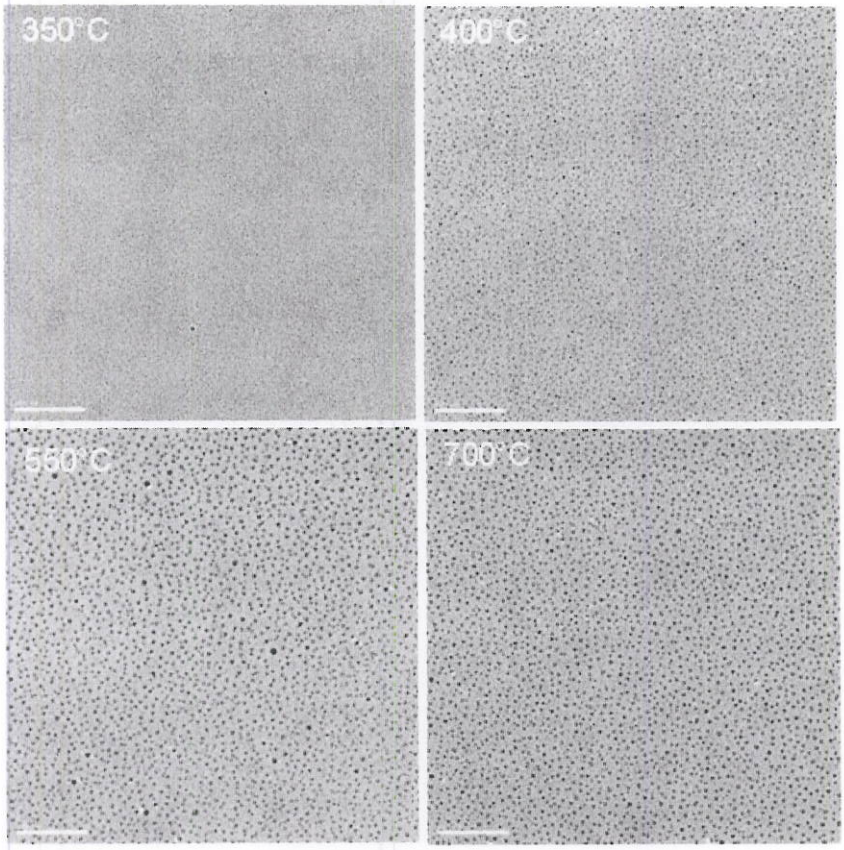

Figure 1.4-4. TEM images of grown Ag nanoparticles, taken at heating temperatures.

PbTe nanotubes are in-situ heated on TEM. Figure 1.4-5 shows the TEM image before and after heating in vacuum. After heated at 400 °C, the corners of PbTe cubes melt. With the heating temperature increases, more portion of the nanocubes evaporate till whole nanotubes disappear.

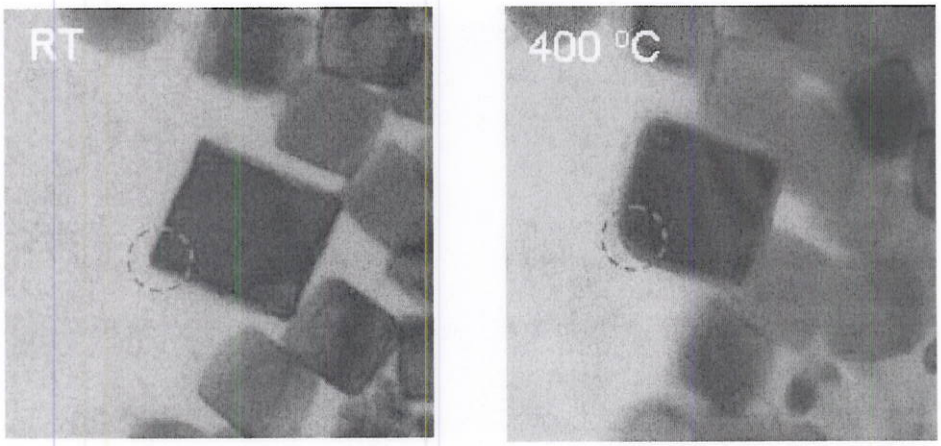

Figure 1.4-5. *In-situ* TEM images of PbTe nanotubes.

The CdSe QDs are heated in vacuum. Figure 1.4-6 shows the morphology of QDs after heated at different temperatures in vacuum. The size decreases with heating temperature.

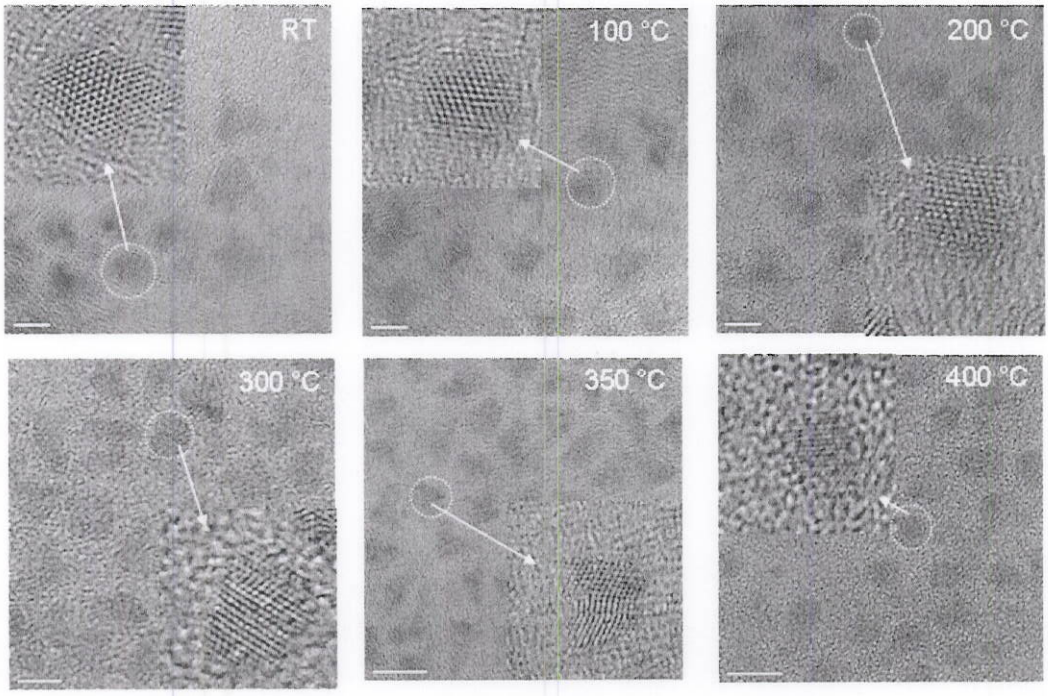

Figure 1.4-6. TEM images of CdSe QDs after being heated in vacuum.

1. 5. Heating of Ag nanoparticles and nanothermometers

Based on the previous experiments, a new kind of nano-thermometer is produced. Below are the details of the thermometer.

1. 5.1. Room temperature observation of Ag nanoparticles heated in vacuum

Ag nanoparticles can be heated up to 1000 °C inside a TEM. The structure changes such as size is monitored as a function of the heating temperature and heating durations.

Suspension containing Ag nanoclusters were deposited on a series of TEM grids. Ag nanoclusters are irregular with a size ranging from 10 to 100 nm (Figure 1.5-1). After heating to a high temperature, smaller silver nanospheres nucleate and grew on the TEM grids. Energy X-ray dispersive spectrum, selected area electron diffraction, and high-resolution TEM (HRTEM) indicated that the nanospheres were Ag nanocrystals.

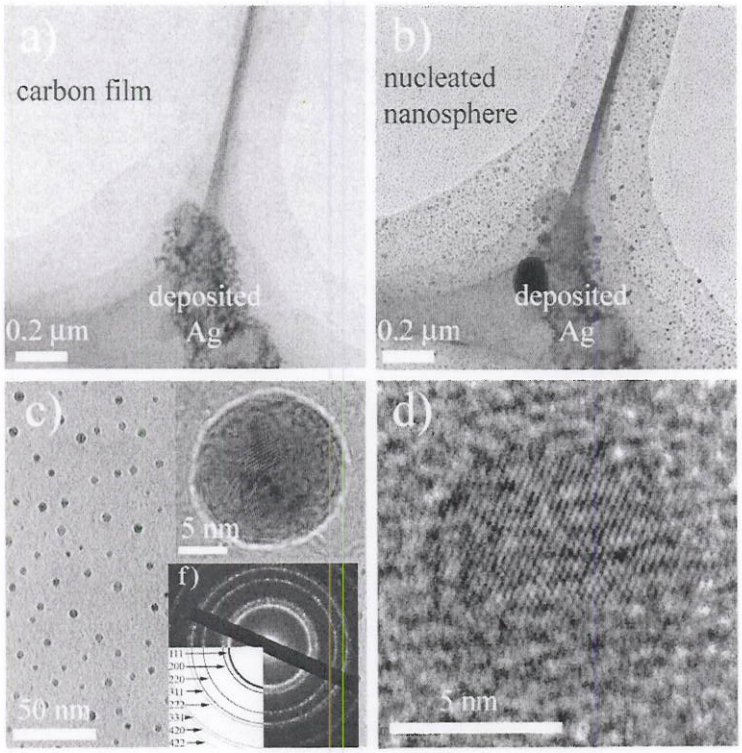

Figure 1.5-1. Room temperature TEM images of (a) Ag nanoclusters before heating, (b) Ag nanospheres nucleated on TEM grids after heating, (c) zoomed Ag nanospheres, (d) HRTEM image of a typical Ag nanosphere. Top inset in (c) is HRTEM image of a nanosphere taken at 500 °C in vacuum. Bottom inset in (c) is selected area electron diffraction of the nanospheres shown in (c).

After heating at high temperature, the nanosphere size increases with increasing temperature. Figure 1.5-2 shows a series of room-temperature TEM images, nanosphere size distribution, and the average nanosphere diameter after heating at different temperatures and cooling down. The nucleated nanospheres are smaller with heating at 300 °C than those at 500 °C. Histogram of the nanospheres indicates that the diameter of most nanospheres is 4 nm after heating at 300 °C and 14 nm at 700 °C.

Quantitative relation between the average nanosphere diameter and the heating temperature is obtained and shown in Figure 1.5-2. The number of nanospheres per unit area (areal density) is also temperature dependent. The areal density of the nanospheres decreases with the heating temperature.

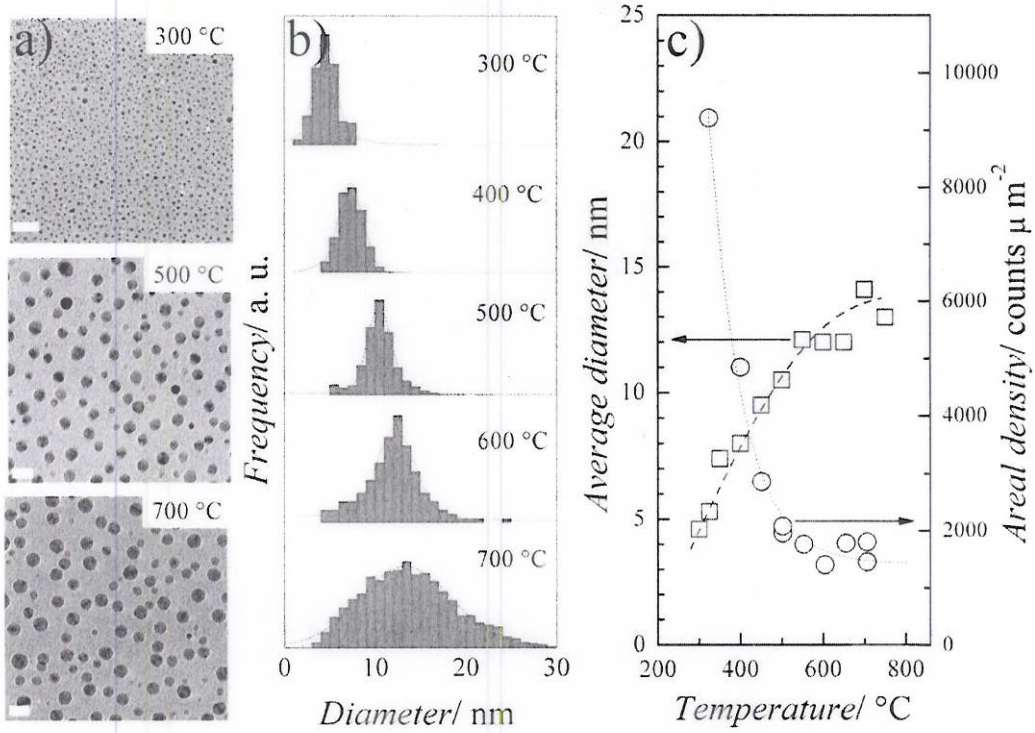

Figure 1.5-2. (a) Room temperature TEM images of nanospheres after being heated at different temperatures (a new sample is prepared for each temperature). The scale bar is 20 nm. (b) Room temperature size distribution of the nanospheres that were heated at different heating temperatures. The distribution is statistically analyzed from thousands of nanospheres recorded on TEM images. (c) Temperature dependent average diameter and areal density measured at room temperature. Rectangles: average diameter; circles: areal density.

5.2 High temperature observation of Ag nanoparticles at heating temperature

In order to study the dynamic behavior of the nanospheres during heating, one sample was heated to 300 °C and held at this temperature for 5 min and observed; then heated to 350 °C and held at this temperature for 5 min and observed, and repeated the procedure at 400 °C, 450 °C, 500 °C, 550 °C, 600 °C, 650 °C, 700 °C, and 750 °C.

Figure 1.5-3 shows three typical TEM images of the nanospheres that were heated at 350 °C, 500 °C, and 750 °C. The size of the nanospheres clearly increases with heating temperature. Figure 1.2-1b shows several histograms of the nanosphere diameter at different heating temperatures. The average diameter is 20 nm at 750 °C, but only 14 nm in Figure 1.5-3, which is the result of the continuous heating and longer accumulative holding time. Figure 1.2-1c shows that the average diameter of the nanospheres increases with the temperature, and the rate of the temperature increase is large from 300 °C to 400 °C, followed by a slower increase in the range

of 500 °C – 750 °C, correspondingly, the areal density decreases rapidly before 400 °C and slows significantly after 400 °C.

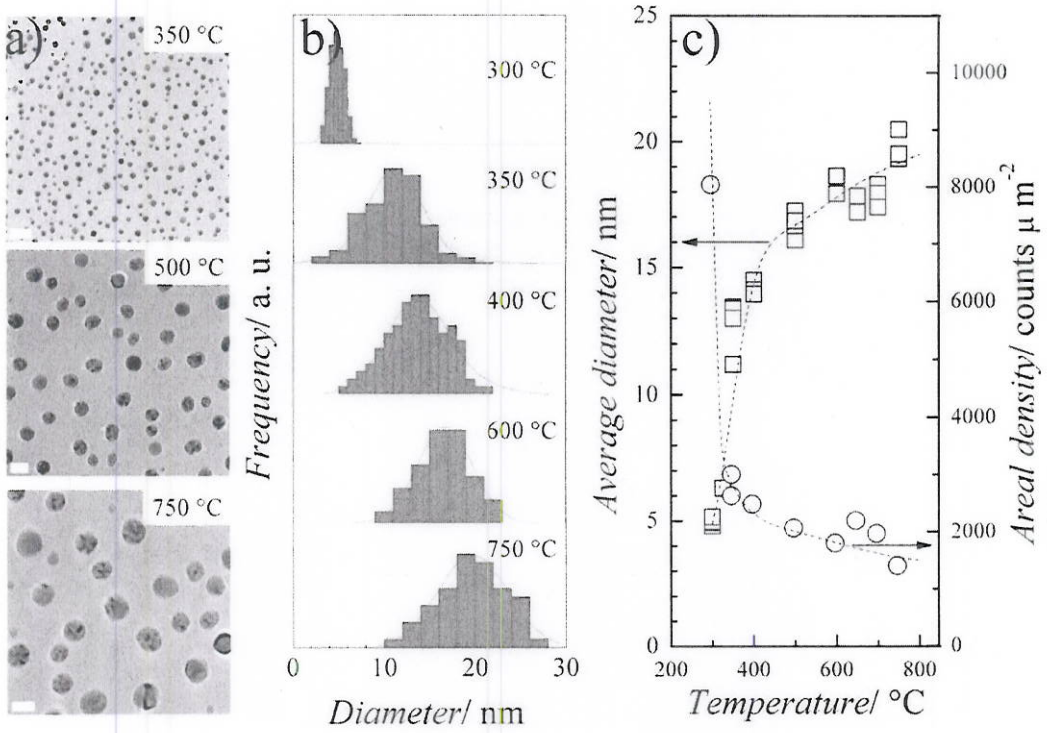

Figure 1.5-3. (a) TEM images of nanospheres taken at different heating temperatures (one sample is used for all the temperatures, and the same experiment was repeated a few times). The scale bar is 20 nm. (b) Size distribution of the nanospheres at the heating temperature. The size distribution was statistically analyzed from thousands of nanospheres recorded on TEM images. (c) Temperature dependent average diameter and areal density measured at the heating temperature. Rectangles: average diameter; circles: areal density.

We took a series of TEM images at heating temperatures (325 °C, 350 °C, 400 °C, 500 °C, 550 °C, 600 °C, 700 °C, and 750 °C) and at room temperature after heating (how it is cooled?). The size distribution of nanospheres at each heating temperature before cooling down to room temperature is analyzed and compared with the size distribution after cooling down to room temperature. Statistical analyses show that the size distribution of nanospheres at room temperature is the same as that at the heating temperature within experimental error, indicating that the Ag nanospheres do not change size during the studied cooling process, which may not be the case if the cooling rate is slow. It means the Ag nanosphere size distribution at high temperature can be preserved to room temperature when they are cooled fast enough, which is normally the case of explosion environment. Two typical TEM images are shown in Figure 1.5-4.

After a size distribution of nanospheres was established at a heating temperature, the diameter of nanospheres does not depend on annealing time below 615 °C. We in-situ heated several nanospheres with diameter of 5 - 20 nm at 400 °C for 2 s, 10 s, 30 s, 1 min, 3 min, and 5 min, respectively. No obvious diameter change is observed.

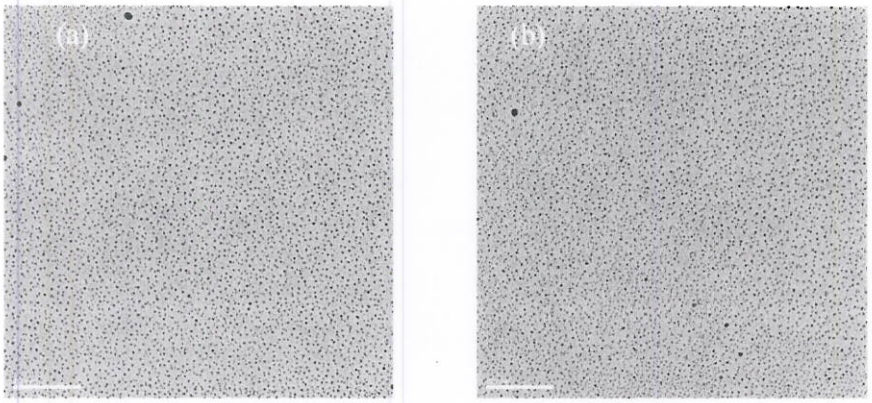

Figure 1.5-4. TEM images of nanospheres heated at 750 °C. (a) Image taken at the heating temperature and (b) image taken at room temperature after cooling down.

1.5.3 Room temperature observation of Ag nanoparticles heated in air

Another heating process was carried out in ambient air condition in order to compare with the heating in vacuum, also to study the oxidation process.

The Ag nanoclustes are heated in air at 300 °C, 400 °C, and 500 °C for 2 s, 10 s, 30 s, 60 s, 120 s, and 300 s. There are two factors affecting the nanosphere size. One is the growth of the Ag nanospheres in air, increasing the nanosphere diameter. Another is the oxidization of the nanospheres, decreasing nanosphere diameter. Figure 1.5-5 shows a series of TEM images heated at 300 °C for different heating time. The nanosphere size increases with heating time firstly (Figure 1.5-5a-e) and decreases after longer heating time (Figure 1.5-5f). Figure 1.3-2 shows the TEM images at different heating temperatures. Obviously, oxidization affects the Ag nanospheres size greatly.

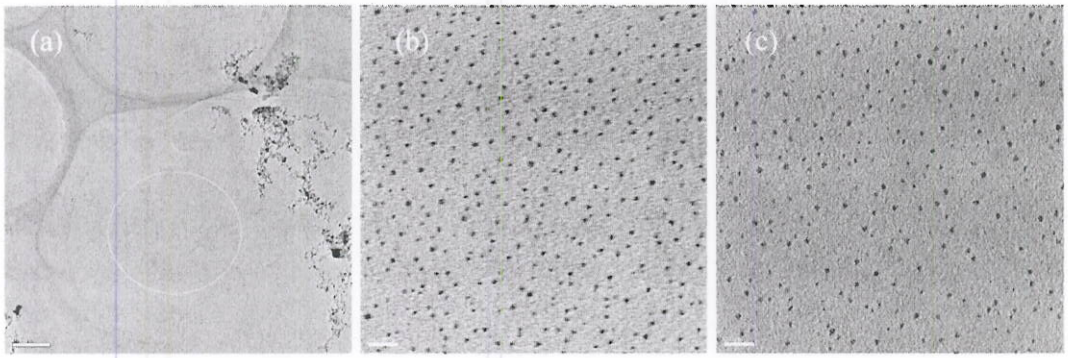

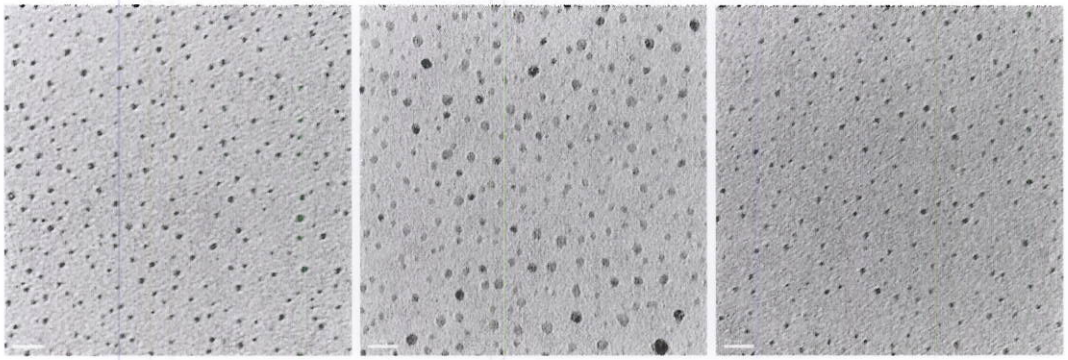

Figure 1.5-5. TEM images of Ag nanoparticles heated at 300 °C in air for (a) 0 s, (b) 2 s, (c) 30 s, (d) 60 s, (e) 120 s, and (f) 300 s.

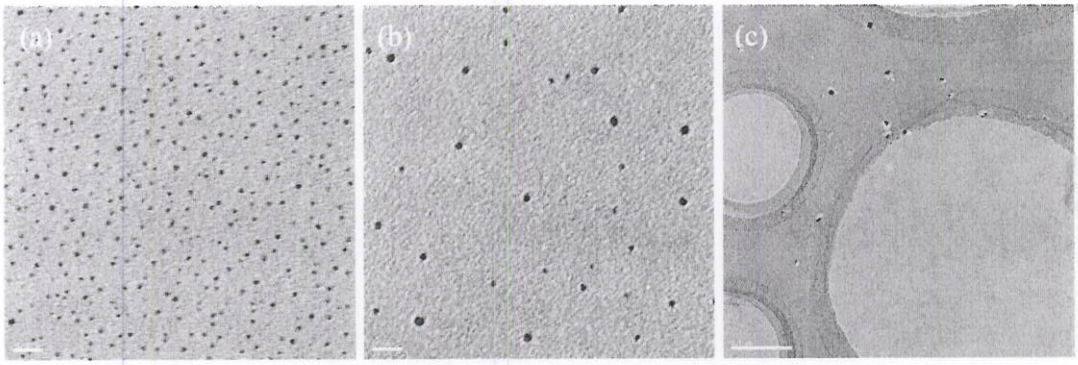

Figure 1.5-6. TEM images of Ag nanospheres heated at (a) 300 °C, (b) 400 °C, and (c) 500 °C for 2 s in air.

1.5.4 Temperature history sensor employing Ag nanospheres

Based on the temperature-dependent size/areal density of nanospheres (Figure 1.5-3), a new type of temperature history sensor can be fabricated using the nanosphere size/areal density as temperature readout. In such temperature history sensors, the individual nanosphere size/areal density records the temperature they experienced, and can be read later at room temperature when the event is over. From this point of view, the new temperature history sensor can work as a traditional mercury-filled medical thermometer, recording the maximum temperature and be read later. This type of temperature history sensor is convenient in some special environment that real-time or in-situ temperature readout/recording is not possible like in the case of explosion. Below is an embodiment shows how to measure a thermal history using the Ag nanospheres.

- **Generation of temperature field in nanoscale**

A temperature field gradient in nanoscale is created by an electron beam combining with a heating TEM specimen holder (Figure 1.5-7). The TEM heating holder generates a uniform

background temperature field T_0 (300 °C). When a new TEM grid with deposited silver nanoclusters is heated inside TEM column under the uniform background temperature field T_0, the electron beam of TEM is focused and radiated on the carbon film coated on the TEM grid, produced an extra temperature gradient with ΔT = 41 °C. The electron beam is controlled to radiate on a small area with a diameter of 300 nm. The electron radiation induced temperature field overlaps over the heating holder produced background temperature field, inducing a temperature field with a higher temperature gradient in nanoscale.

Ag nanospheres are employed to record the nanoscale temperature gradient, in order to explore the application of the Ag nanosphere in temperature history sensors.

- **TEM investigation of Ag nanospheres in temperature field gradient**

Ag nanoclusters were deposited on a TEM grid, heated in the temperature field gradient shown as in Figure 1.5-7 in TEM. After heating, the sample was cooled down to room temperature for TEM observation. Figure 1.5-8 is a room temperature TEM image of the nucleated nanospheres deposited on TEM grid after experiencing the temperature field. The dashed circle marks a higher temperature region (region II, about 41 °C higher than the surrounding region I with a uniform temperature of 300 °C) produced by electron radiation.

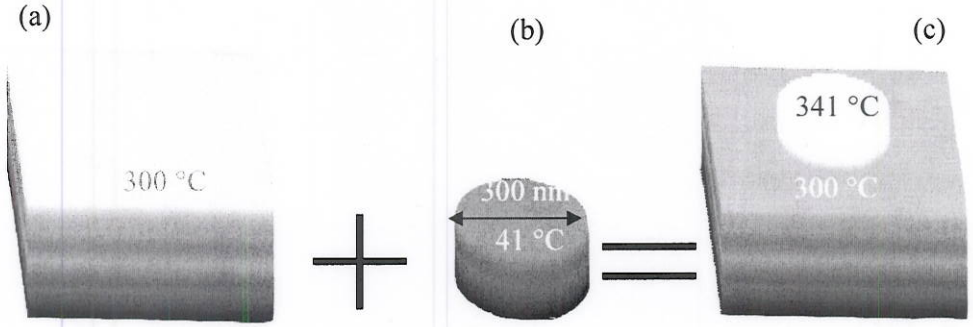

Figure 1.5-7. Generation of a temperature field gradient in nanoscale. (a) A uniform macroscopic temperature field (T_0 = 300 °C) produced by a TEM heating holder. (b) A microscopic temperature field produced by electron radiation (ΔT = 41 °C). (c) A temperature field gradient combining (a) and (b).

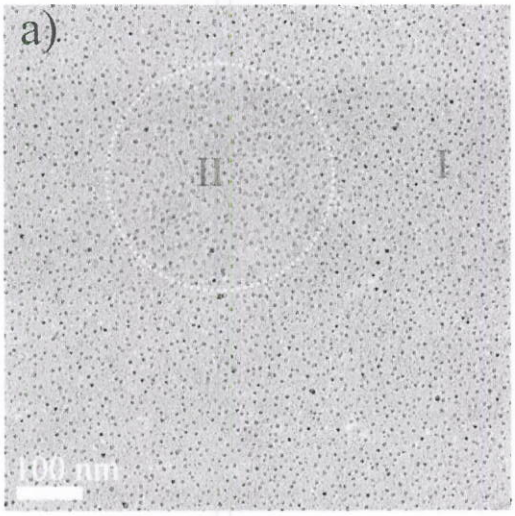

Figure 1.5-8. Room temperature TEM image of Ag nanospheres heated in the temperature field with a temperature gradient shown in Figure 1.5-7. The dashed circle marks the electron radiated region where the temperature is higher ($\Delta T = 41$ °C).

- **Temperature history detection from TEM images: method 1**

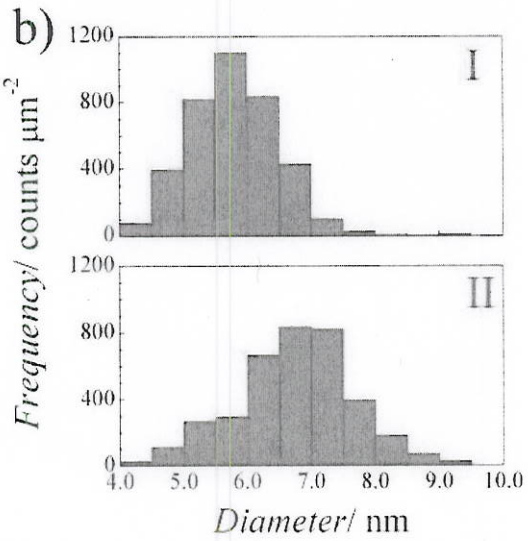

Figure 1.5-9. Ag nanosphere size distribution in regions I and II shown in Figure 1.5-8.

The nanospheres nucleated in region II (higher temperature region) is bigger than those nucleated in region I (lower temperature region). The average diameter calculated from statistical analyses is employed to determine the temperature each region experienced. Figure 1.5-9 illustrates the size distribution of the nanospheres in regions I and II. The average nanosphere diameter is 5.5 nm in region I and 7.0 nm in region II. According to the temperature-dependent diameter curve in Figure 1.5-3c, the average temperature of the radiated region II should be 367 °C and 325 °C in region I. The measured temperature difference $\Delta T = 42$ °C is in

very good agreement with the theoretical value, $\Delta T = 41$ °C. In this method, a temperature gradient within a spatial resolution of 0.07 μm^2 is determined.

1.5.5. Temperature history detection from TEM images: method 2

The temperature history can also be detected from the areal density of nanospheres. As shown in Figure 1.5-6, the nanosphere areal density of the higher temperature region II is lower than that of the lower temperature region I. According to the temperature-dependent areal density curve in Figure 1.5-3, the temperature of the radiated region II is 48 °C higher than that of the region I. The value of temperature rise caused by electron radiation is in agreement with the values measured from above two methods and the theoretical value.

- **Two-dimensional temperature field detected from TEM images**

The two-dimensional temperature field shown in Figure 1.5-10 can be determined using Ag nanospheres. The size of each individual nanosphere in Figure 1.5-8 is measured and the diameter is converted to the corresponding temperature according to the temperature dependence of nanosphere size shown in Figure 1.5-3. Here we assume that each individual nanosphere records the highest temperature it experienced, working as an individual temperature history sensor.

Figure 1.5-10 shows the recorded two-dimensional temperature field reconstructed from the room temperature TEM image shown in Figure 1.5-8. The measured temperature field gradient is very similar to the designed one shown in Figure 1.5-7. A higher temperature region with a diameter of 300 nm is detected and a temperature gradient is observed around the electron radiation region. The two-dimensional spatial distribution of the temperature field is shown as the bottom contour in Figure 1.5-10. The detail of the two-dimensional temperature gradient is recorded with a high spatial resolution. The spatial resolution of temperature determination is controlled by the distance between neighboring nanospheres, related to the nanosphere size and nanosphere areal density. In this case the spatial resolution of the temperature detection is 264 nm^2, i.e., ~16 nm resolution in linear dimension.

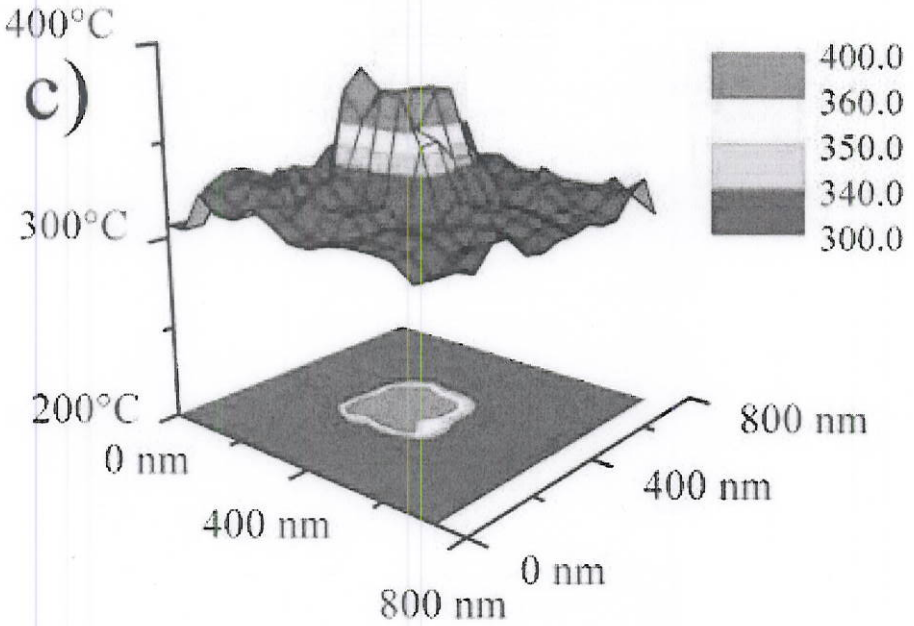

Figure 1.5-10. Recorded two-dimensional temperature field gradient reconstructed from the TEM image shown in Figure 1.5-8.

2 PHOTOLUMINESCENCE STUDIES

In the previous years, the PL of core/shell CdSe/ZnS QDs in size of ~ 5 nm showed strong dependence on their temperature history. The PL could be detected after sample was heated up to 800 °C in a range of seconds of heating times. The quenching of PL intensity and blue-shift of the PL spectra with increasing temperature and heating time provides an optical route to read out the thermal history. We have also carried out more detailed data analysis and using simplified quantum confinement and mass diffusion model to describe the PL property changes. By using PL peak shifting and intensity decay characteristics, the thermal history for a single thermal event could be recorded and retrieved. The time response of QDs sensors has been investigated. The preliminary data show that the QDs sensor in size of ~5 nm has time responses in milliseconds region. Studies related to fundamental properties were also carried out. The following gives a more detailed summary of our results.

2.1 Experiment Setup for Optical Studies

We added a few new components to the original experimental setup as described in followings.

2.1.1 Optical System

As shown in Fig. 2.1.1, the optical system is capable of obtaining both micro-Raman and PL. Excitation sources are extended from continuous wave of green 532 nm to blue 403-410 nm blue laser diode, and 200-400 fs pulsed excitation tunable from 390-430 nm from frequency doubled Ti:Sapphire laser. These excitation sources are necessary for QDs which have wide emission spectral range by their sizes. The pulsed source delivers more excitation energy each pulse to generate excessive electron hole pairs in QDs so that fundamental studies such as electron-phonon interactions in higher energy level and high excitation density region can be carried out. At the same time, pulsed excitation could be used to avoid the optical excitation induced the heating. The QDs surrounding media and pressure can be controlled by a newly adapted sample chamber. A platinum wire driven by a pulsed power supply is used as a temporal heating source. The advantage of the wire heating will be discussed in following section.

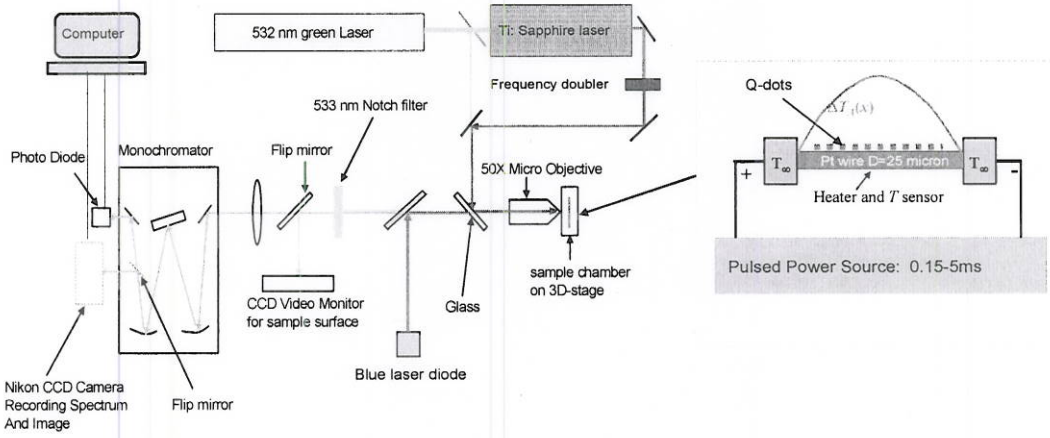

Figure 2.1-1 Experimental Set

2. 1.2. Fast heating using platinum Wire

We use 25 □m diameter and ~1 cm platinum (Pt) wire to mimic fast heating that occurs during extreme thermal events such as explosion. This platinum wire serves both as a heater and sensor since platinum exhibits linear temperature coefficient of resistance (TCR) and provides very good temperature sensitivity. CdSe/ZnS core/shell type of quantum dots with average diameter of ~5 nm are delivered on the surface of wire using a syringe system. A Keithley power source meter that can provide current pulses between 0.1-5 ms is used to supply electric currents across the wire. This Joule heating causes a temperature rise, and hence an increase in electrical resistance of the wire. The electrical resistance of wire is determined using 4-point sensing and with an accurate knowledge of TCR for Pt, we are able to determine the average maximum temperature of the wire during electrical heating.

We solder ~1 cm long Pt wire to two large pads of our sample holder as shown in Figure 2.1.-2 First, we calibrate the wire by passing 5 ms long current pulses of different magnitude and measuring resistances. The average temperature for a given amount of current is then calculated using the known temperature-resistance plot for platinum. Therefore, we know how much current is required to generate a certain temperature within the wire, and hence the quantum dots. We notice that for a wire of ~1 cm length, we may generate temperatures as high as ~700 °C by passing currents of ~1.5 A. PL spectrum is collected using home-built PL setup as shown in Figure 2.1.-2.

To test the Pt wire setup, we heat wire to different temperatures by passing corresponding amounts of electrical currents. Figure 2 shows PL photographs that are obtained from quantum dots that were at room temperature and the ones that were heated to 300 °C and 475 °C. We observe no significant PL shift until 300 °C. However, for temperatures higher than 300 °C, we observe a clear trend of blue-shift in PL spectrum with increasing temperature as shown in Figure 2.1.-3 and 2.1.-4. These results demonstrate that thin platinum wire is a good platform to conduct fast heating experiments. These results again confirm that there is a certain energy barrier associated with these quantum dots that needs to be overcome to initiate mass diffusion process.

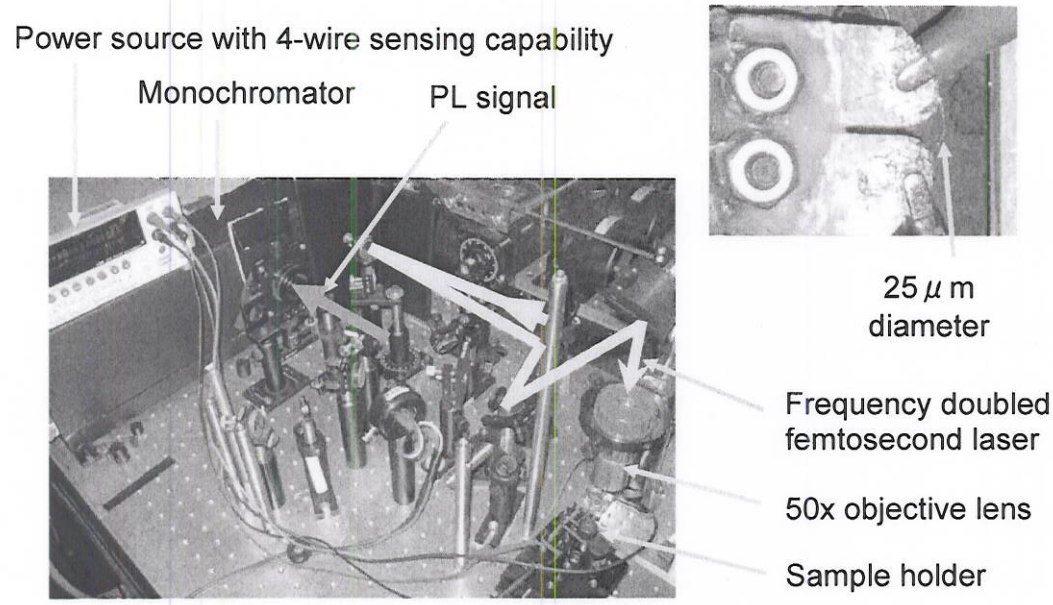

Figure 2.1.-2: Home-built photoluminescence system. The setup has provision for using three different laser lines: 403-410 nm blue laser diode, 532 nm green pump laser to Ti:sapphire femtosecond laser and 390-430 nm blue laser output by frequency doubling Ti:sapphire femtosecond laser. The laser light is focused onto the sample using an objective lens. The typical spot size is on the order of a few microns. The reflected light that includes our signal of interest i.e. PL signal is then allowed to pass through the slit of a monochromator (MC). As this light further passes through mirrors and gratings inside the MC, it is spatially separated and collected by a CCD digital camera. The figure on the top-right corner shows the sample holder along with the platinum wire that is attached to two large metallic pads. 4-point sensing is used to accurately measure the resistance of wire. A Keithley power source meter is used to supply electric current pulses.

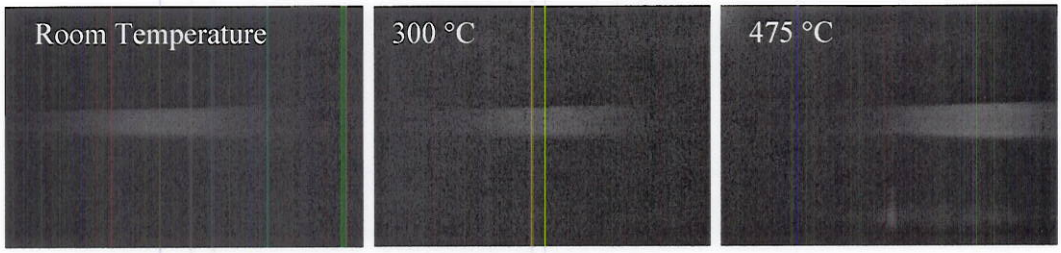

Figure 2.1.-3: CCD snapshots of PL signal from ensemble of quantum dots that were i) unheated (25 °C), ii) heated to 300 °C and iii) 475 °C. These quantum dots were dispersed on a 25 μm diameter Pt wire. The horizontal and vertical directions on these CCD images correspond to wavelength and position, respectively. There is no significant shift in PL spectrum from room temperature to 300 °C, although a large blue-shift is observed for 475 °C sample.

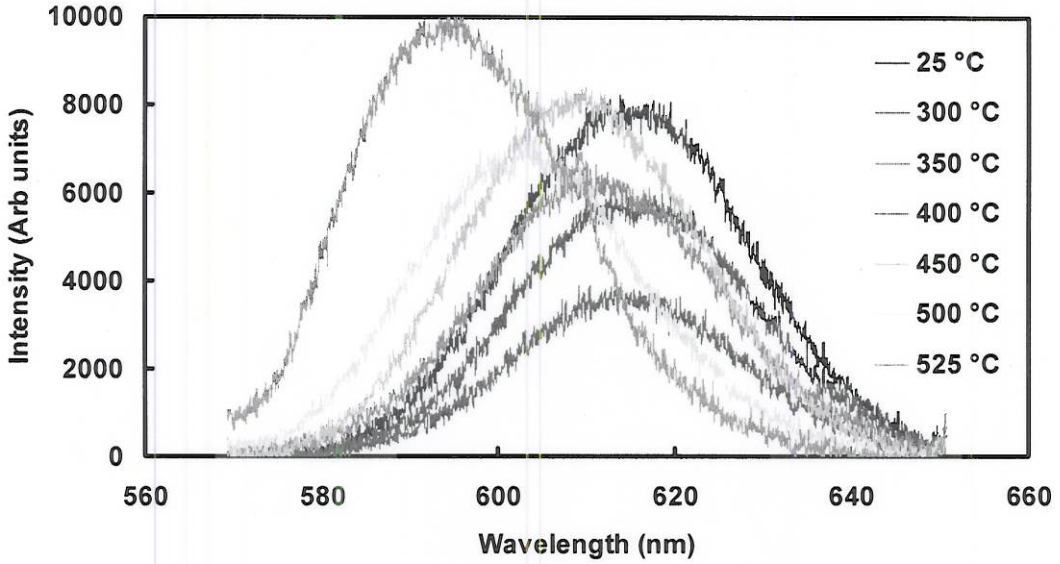

Figure 2.1.-4: PL spectrum from ensemble of quantum dots that were heated to different temperatures. These quantum dots were dispersed on a 25 μm diameter Pt wire. There is no significant shift in PL spectrum between 25-300 °C. After 300 C, PL peak wavelength begins to shift towards blue spectrum. Note that since quantum dots are not uniformly distributed on Pt wire and the fact that the measurement location moves for each temperature setting, intensity does not follow a descending trend with temperature.

2.1.3. Heat transfer model for quantum dot heating

A simple fin model is used to describe the heating of wire by passing a pulsed electric current and subsequent cooling in ambient environment. The energy balance equation is as follows

$$\rho c_p A \frac{\partial T}{\partial t} = kA \frac{\partial^2 T}{\partial x^2} + Aq''' - \bar{h}P\left(T - T_a\right) \quad (1)$$

$$q''' = \frac{I^2}{A^2}\rho_R \quad (2)$$

$$\rho_R = \rho_{R0}\left(1 + aT + bT^2\right) \quad (3)$$

Here ρ, C_p, k, A, p, ρ_{R0} are density, volumetric heat capacity, thermal conductivity, cross-sectional area, perimeter, electrical resistivity at 0 °C of the Pt wire, respectively; I, h, T_a are the electrical current, heat transfer coefficient, ambient temperature, respectively.

Using equations (1), (2), (3) and resistance-temperature plot for Pt wire, we are able to extract equivalent heat transfer coefficient of the environment. Figure 4 shows that h for the environment is very high and linearly increases with temperature. The heat transfer coefficient for natural convection and radiation processes can not explain such high h. This suggests that phase change processes such as boiling may be occurring during heating. This scenario is

possible considering high temperatures, humid environment and presence of traces of liquid toluene on wire.

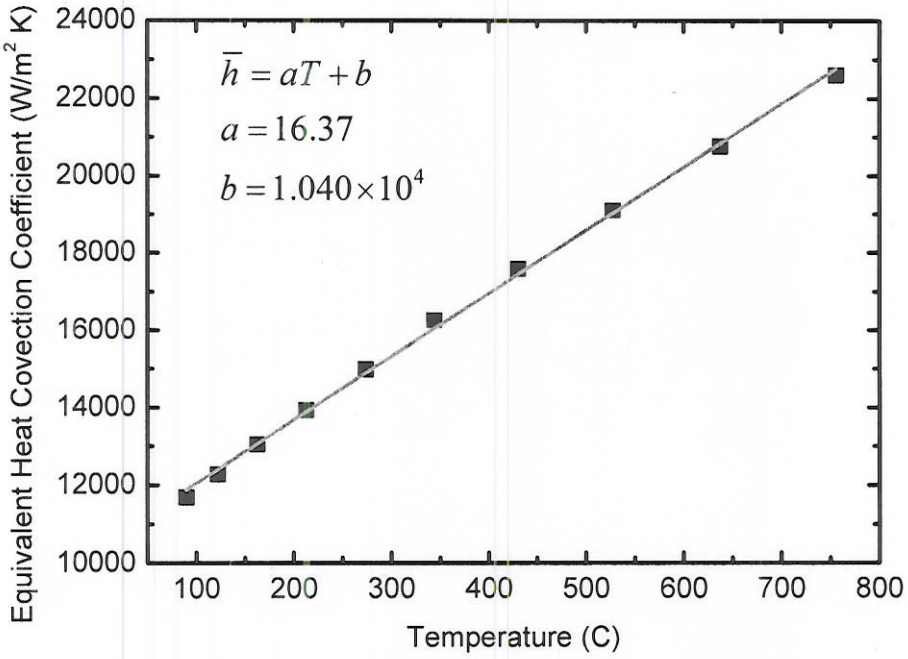

Figure 2.1.-5: Equivalent heat transfer coefficient as a function of wire temperature.

2.1.4. PL along the length of the wire

We measure PL peak wavelengths from ensemble of quantum dots that were placed at three different locations on the wire: center of the wire, and 0.6 mm and 3 mm from edge of the wire. These quantum dots were heated for 5 ms. The results are summarized in Figure 5 as a function different maximum temperatures. It is observed that PL peak wavelength does not shift until ~300 °C for all three locations. After 300 °C, there is a clear blue-shift in peak wavelength for all three locations. For a given maximum average temperature, it is noticed that center of the wire exhibits largest shift followed by 0.6 mm from the edge location. The location that is 0.5 mm from edge displays smallest shift in peak wavelength. This suggests that electrical heating establishes a parabolic temperature field where temperature increases from edge to the center of the wire.

Applying heat transfer coefficient values as determined in previous steps into energy balance equation, we may plot temperature evolution along the entire length of the wire. Figure 6(a) and (b) show evolution of temperature when passing currents of 1.096 and 1.313 A, respectively. We notice temperature near the edges is lower compared to center of the wire, confirming our hypotheses and results of Figure 5. We also calculate the maximum temperature on three locations and plot them in Figure 8(a). Although we notice a general trend that PL shift increases

with increasing maximum temperature, yet it seems it is not the only factor. Since mass transport across core/shell interface is a diffusion process, both the time and temperature are important. Therefore, we need to calculate area under the time-temperature plot. It is also to be noted that since no mass diffusion occurs until 300 °C, we may ignore area below 300 °C. In Figure 8(b), we plot PL shift as a function of time-temperature integration area. We find that for the same time-temperature integration area, the blue-shift in PL peak wavelength appears to be the same for different locations on the wire. This confirms that temperature induced mass diffusion process in quantum dots is a function of both time and temperature i.e. temperature history.

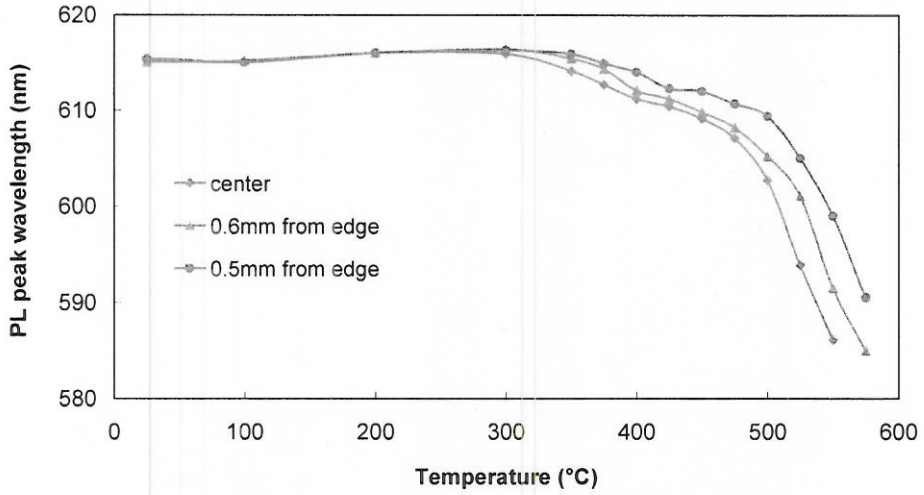

Figure 2.1.-6: Blue-shift in PL as a function of average maximum temperature of the wire for three different locations on the wire.

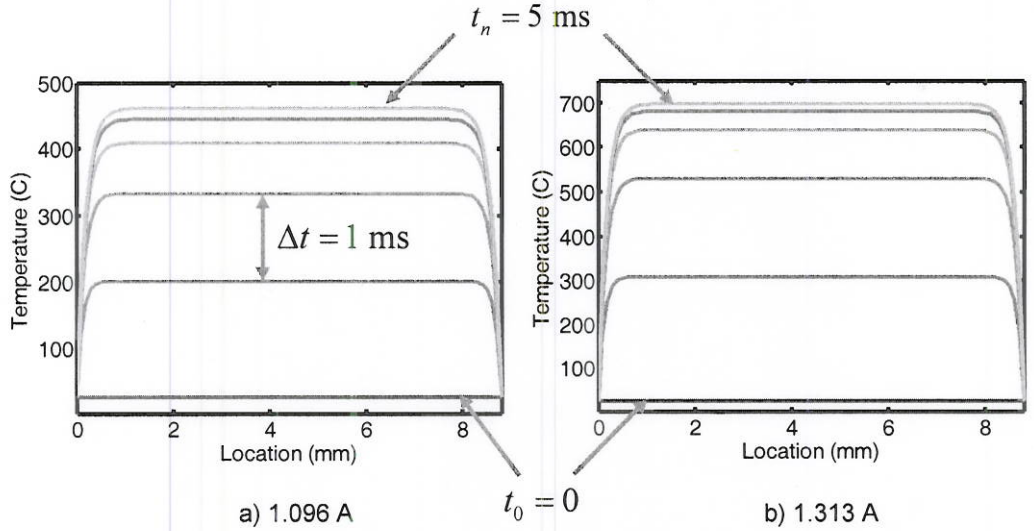

Figure 2.1.-7: Evolution of temperature during fast heating of Pt wire for two different values of electric current: (a) 1.096 A, (b) 1.313 A. The current pulse in ON for 5 ms. It is to be noted that the higher current results in higher maximum temperature in the wire.

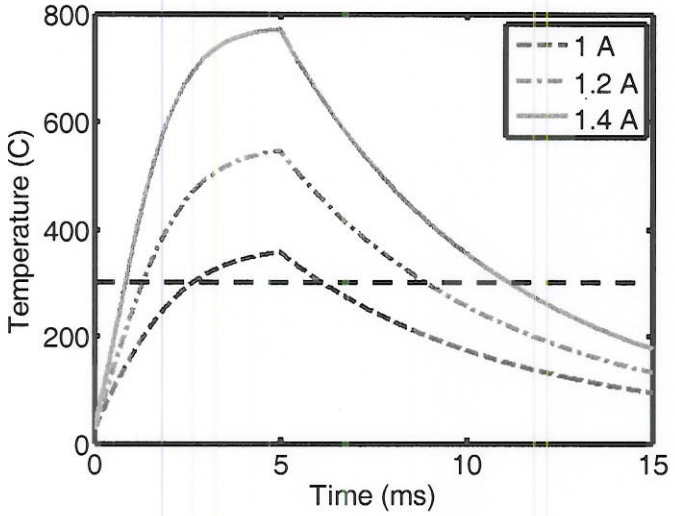

$$t_{300} = \int_{T>300} (T - 300)\, dt$$

Figure 2.1.-8: Temperature profile at the center of the wire during heating and cooling of Pt wire. For calculating area under time-temperature curve, we neglect area below 300 °C as no mass diffusion is observed until 300 °C.

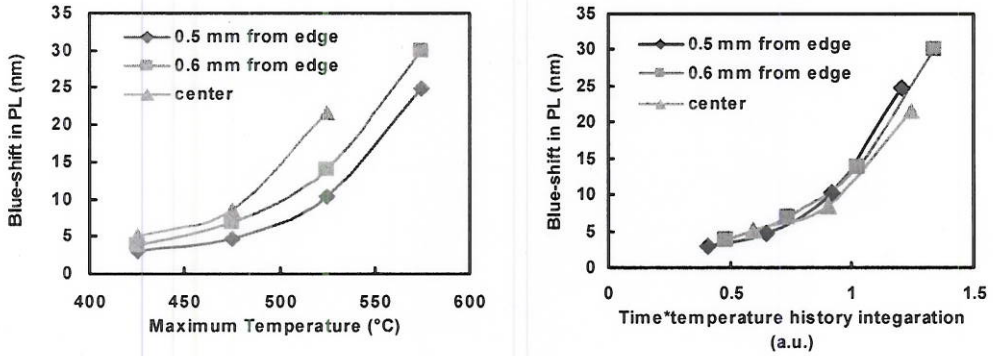

(a) (b)

Figure 2.1.-9: For three different locations on the wire: (a) Blue-shift in PL as a function of maximum temperature, (b) Blue-shift in PL as a function of area under time-temperature curve.

2.2 Slow Heating Response and PL Data Analysis

In the 2008 report, we showed the slow heating PL data of CdSe/ZnS QD data. We continued this year the data analysis. Figure 2.2-1 shows the temperature dependent PL spectrum of the QDs after thermal annealing (shown in year 2008 report). The sample was heated for 10 seconds on a hot plate in ambient air, and removed to a cold metal plate for reducing residual heating. The spectrum was obtained after the sample was cooled to room temperature. A series of temperatures up to 450 °C were tested as indicated in the figure. As seen in Fig. 2.2-1a, PL

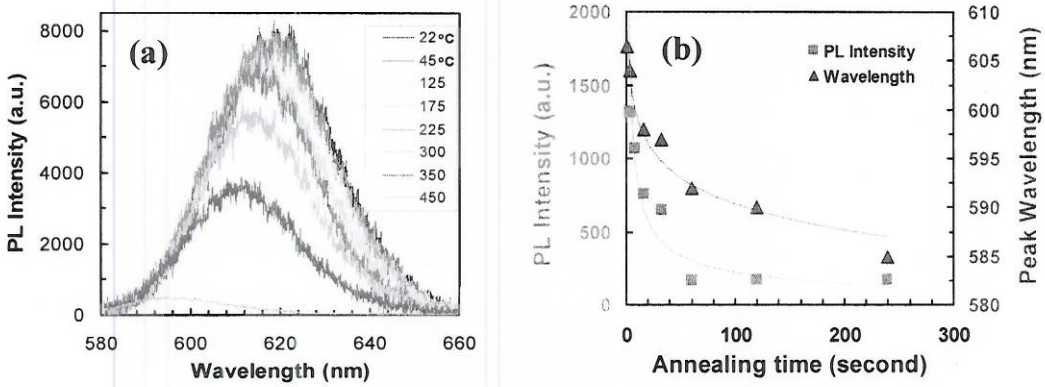

Figure 2.2-1 a) PL spectrum of thermally annealed CdSe/ZnS nanocrystals of ~5 nm. Each spectrum was recorded at room temperature after 10 s annealing at a series of temperatures up to 450 °C as indicated. b) The PL peak shift (triangles with guideline) and intensity decay (squares with guideline) with annealing time period at the fixed temperature of 410 °C.

signals are readily detectable with the heating temperature up to 450 °C. Below 150 °C, the PL peak wavelength and intensity changes very little. Between 150-450 °C, the PL peak exhibits the blue shifting with increasing annealing temperature. At the meantime, the PL intensity also decays with increasing heating temperature due to the defect creation that quenches the luminescence. Both PL peak shift and intensity decay provide the fingerprints of irreversible structural changes during the thermal exposure that the QDs experienced. The sensing range of the temperature depends on the size of QDs used. For this 5 nm QDs, the PL can be detected after 10 seconds annealing up to 800 °C as shown in the report before.

With the similar procedure in temperature-dependent studies, Fig. 2.2-1b shows the thermal annealing time dependent behavior of the QDs heated at 410 °C. The peak wavelength and the intensity data were collected from the PL spectrum. By performing the annealing time dependence at a set of temperatures, history fingerprints can be mapped out in a targeted sensing range of both temperature and time so that the time-temperature response of the QDs during annealing processes can be fully characterized.

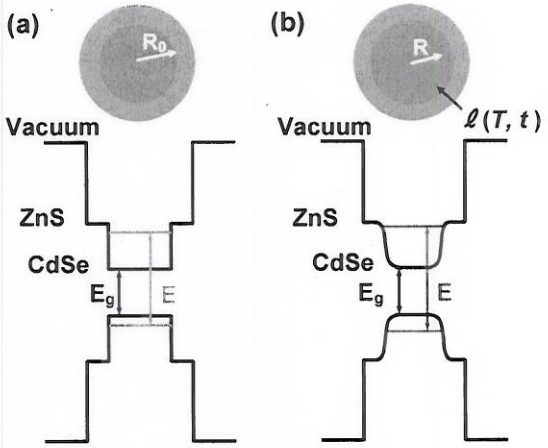

Figure 2.2-2 Illustration of the energy band diagram of a core/shell CdSe/ZnS QD before (a) and after (b) thermally induced mass diffusion at interface between CdSe and ZnS.

The PL peak wavelength shift could be ascribed to the size effects induced by the mass diffusion. The quantum confinement energy of a QD depends strongly on its

size and the surrounding energy barrier. The thermal mass diffusion at the interface of the constituent materials induces the size and shape changes of the energy well and the barrier, which is illustrated in Fig. 2.2-2. The confinement energy E with the core radius R_0 of a QD is approximately as $E = \hbar^2 S_h^2 / 2mR_0^2$, S_h is a geometric factor. After the thermal mass diffusion, the energy change with diffusion length ℓ can be expressed as $\Delta E = \hbar^2 S_h^2 \ell / mR_0^3$ in the first order approximation. The mass diffusion length ℓ is proportional to $\sqrt{Dt}$ with diffusivity $D = D_0 \exp(-\frac{E_b}{k_B T})$, where E_b is the energy barrier of the diffusion, and k_B is the Boltzmann constant. Finally, the mass diffusion induced energy shifting with temperature T and time t described as

$$\Delta E(T,t) = \frac{\hbar^2 S_h^2}{mR_0^3}\sqrt{D_0 t}\exp(-\frac{E_b}{2k_B T}) \qquad (4)$$

The energy barrier E_b and the diffusivity D_0 can be determined by fitting the experimental data. Equation (4) indicates that the energy shift induced by mass diffusion in the QDs follows Arrhenius-type kinetic process, and is very sensitive to the size. The temperature-dependent PL peak shifting data in Fig. 2.2-1a and time-dependent PL data in Fig. 2.2-1b were plotted in log-scale as shown in Fig. 2.2-3(a) and (b). Fitting the temperature dependent data of Fig 2.2-3(a) by Eq. (4), the diffusion barrier E_b is about 0.7 eV, and the diffusivity D_0 is around $1.6\text{x}10^{-18}$ m^2/s that falls within the reasonable range of self-diffusivity value. However, the time dependence follows $t^{0.27}$ instead of $t^{0.5}$ as predicted in Eq. (4). The temporal temperature responses of equation (4) can be simplified as $\Delta E = E_0 t^{\alpha} \exp(-\frac{\varepsilon}{T})$ so that the thermal process could be characterized by parameter α and ε, which are determined by simulating the thermal process of

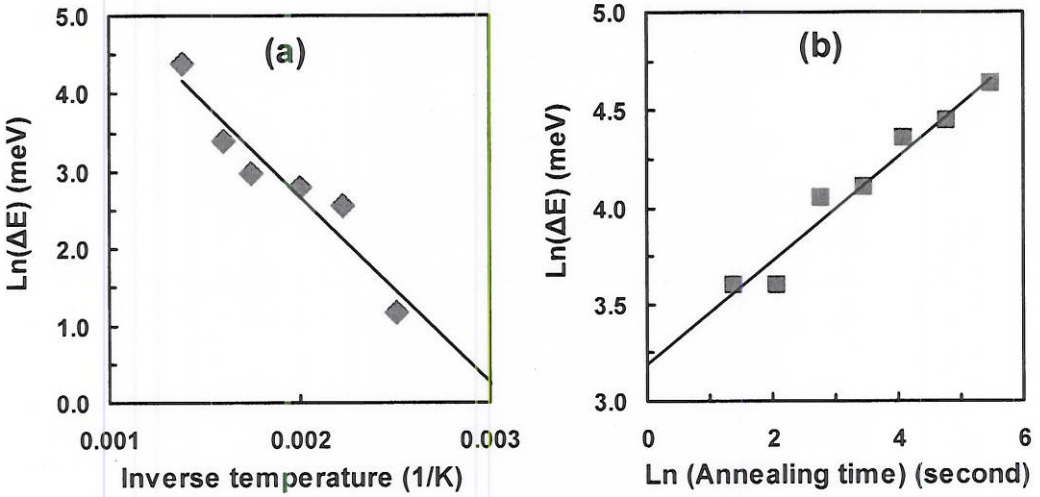

Figure 2.2-3 Emission energy changes ΔE with (a) annealing temperature and (b) annealing time.

the targeted environment to be measured by the QD sensors.

A thermally induced emission energy change of the sensor in a short time at high temperature might be equivalent to the change in a longer time at a lower temperature. This non-uniqueness is a challenge for thermal history recording and data retrieving. In most application cases, both temperature and evolution time are unknown factors in a single thermal event, and both information need to be recorded and extracted later. The lack of uniqueness could be compensated by using a second, or even a set of sensors which has different response rates. With more sensing units applied, more history could be recorded and retrieved. As shown in Fig. 2.2-1, the PL intensity also changes with the thermal exposure in addition to peak wavelength, which could be used as a second sensing signal. Hence, for the same thermal event, the PL QD sensor can provide two independent fingerprints. The PL intensity decay during thermal annealing is proportional to the defect generation rate □, which is expected to follow the Arrhenius-type kinetic process as well. The intensity change ΔI with annealing temperature and time can be generally expressed as

$$\Delta I(\gamma) = \gamma_o t^{\alpha} \exp\left(-\frac{E_a}{k_B T}\right) \tag{5}$$

where E_a is the thermal activation energy for the defect generation, and γ_0 represents the defect generation rate before the annealing. The parameter α characterizes annealing rate with time. The intensity dependence data from Fig. 2.2-1 are plotted in log-scale as shown in Fig. 2.2-4(a) and 2.2-4(b). The intensity decay could be described by Eq. 5 with the defect activation energy E_a of 0.27 eV, and α of 0.06. Comparing with emission energy dependence by mass diffusion with 0.7 eV of energy barrier and 0.27 of α, these two processes have very distinguished characteristics. The thermal processes of $\Delta E\ (T, t)$ and $\Delta I\ (T, t)$ described by Eq. (4) and Eq. (5) in one sensor have advantages over multiple sensors which might be required to clarify the equivalency of the temperature and time in a thermal event, to narrow down the uncertainties in retrieving recorded temporal information, and to record and retrieve more information in a thermal event.

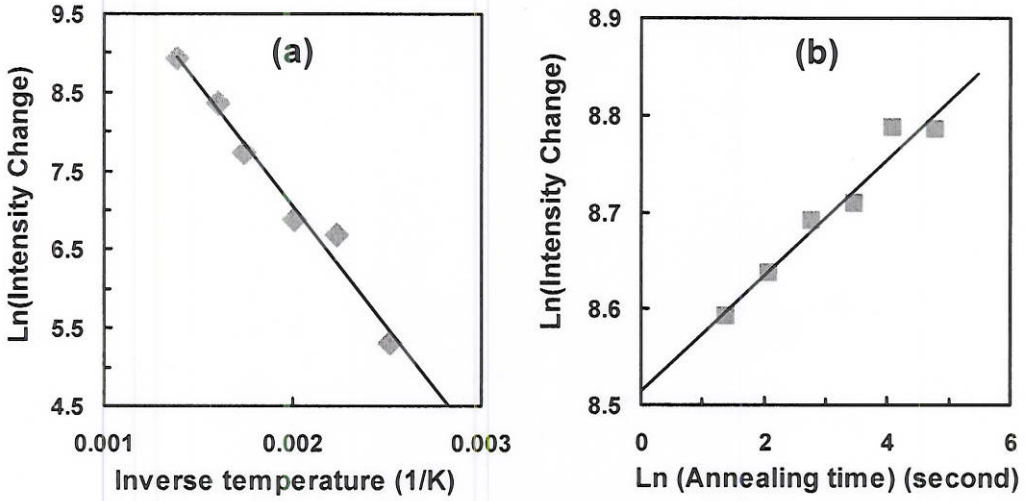

Figure 2.2-4 Emission intensity changes ΔI with (a) annealing temperature and (b) annealing time.

2.3 Fast Time Response of Quantum Dots Sensor

Since optical emission energy of QDs has strong dependence on their size, a small change of size and shape induced by thermal mass diffusion will result in PL change. The high thermal sensitivity of QDs in both exposure time and temperature is expected. The same sized QDs that were tested in longer heating time before are used for shorter pulsed heating. The Pt wire and pulsed power source were used as heating source. The PL Data were obtained by pulsed blue excitation as described in previous section. In this study, the QDs of 5 nm are directly dropped on the center of Pt wire, the heating pulse profile of the wire is around 30 milliseconds after 2 milliseconds current pulse. The temperature were controlled by driving current, and estimated by wire resistance. Figure 2.3-1 shows PL spectra at the heating temperature ranged from 325 °C to 493 °C. In comparing with the PL spectra excited by low intensity excitation of green 532 nm laser, which shows symmetric spectral shape centered around 620 nm at room temperature (Fig. 2.2-1a), the spectrum under pulsed excitation exhibits two band structure which could be ascribed to the band filling due to low emission rate of lowest energy transition level. The low emission rate can be described by so called "dark exciton" or localized exciton by traps and defects. The PL mechanism of such QDs remains unclear, and even after lots of investigations. Nevertheless, PL peaks and shapes show strong dependence with annealing temperature in tens of milliseconds range. A single band emission from lowest dark exciton emission can be obtained using weak continuous wave laser, which help the data analysis. The emission energy band of higher exciton states can be used as a new thermal recording fingerprint, and could be further studied. The shifting is more drastic than longer heating time data obtained before. Mechanisms of such differences are under investigation..

2.4 Other Preliminary Studies

2.4.1 Optical Property Studies

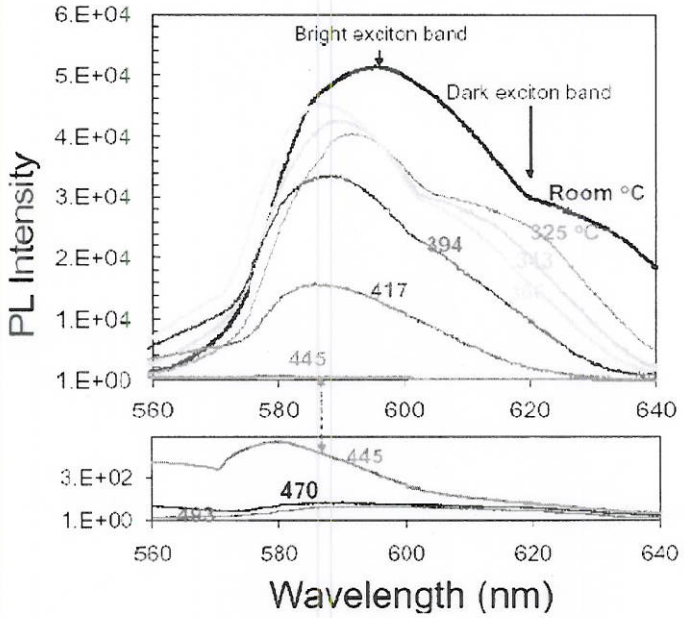

Figure 2.3-1 PL spectrum of 5 nm CdSe/ZnS quantum dots heated on Pt wire by 2ms pulsed current. Temperature of the wire decays in about 30 ms. PL was obtained by 200 fs blue laser.

To further test the band filling or saturation effects obtained under the pulsed excitation, the same QDs were studied by using continuous wave of 532 nm laser at several excitation intensity levels. The results are shown in Fig. 2.4 -1. At low excitation intensity, the spectrum is a single band as obtained before (Fig. 2.2-1). When excitation intensity increases about 10 times, the band filling appears and lower energy band trends to be red shifted. At even higher excitation level, the higher energy emission starts dominant as observed in pulsed excitation studies. Such low saturation level is generally not observed in quantum well structure even with very strong pulsed excitation. The results further indicate that the lowest emission band is from "dark exciton" or localized exciton. The red shifting of emission peak is generally from two main reasons. One is high excitation induced heating leading to bandgap shrinking. It is strongly possible when condenser such as micro-objective were used. Another is from many body effects at high excitation intensities. The two processes can be identified by pulsed excitation at very low intensity level, and more careful studies are required.

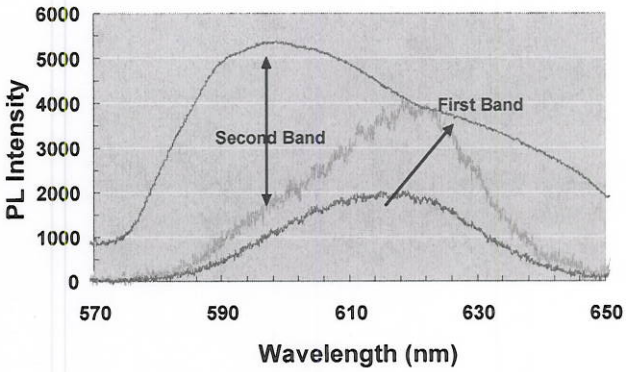

Figure 2. 4 -1 Excitation intensity dependence of ~5 nm QDs under continuous wave of 532 nm laser. PL intensity is not normalized in order to compare PL peak.

2.4.2 QDs with the Size of ~2 nm

Smaller QDs are more sensitive to their size and shape change by thermal mass diffusion. Nominal size of ~2 nm has emission peak around 510 nm as shown in Fig. 2.4-2. At lower heating temperature, the PL peak blue-shift as expected. At higher temperature, PL from smaller dots in multi-dots clusters is quenched or burned out as observed in large dots at much higher heating temperature and longer heating duration. The data indicates higher sensitivity of small dots as expected. However, these are preliminary testing results. The temperature readings on both hotplate and the wire are not accurately determined. More detailed studies are required before reaching to the conclusion about the size sensitivity.

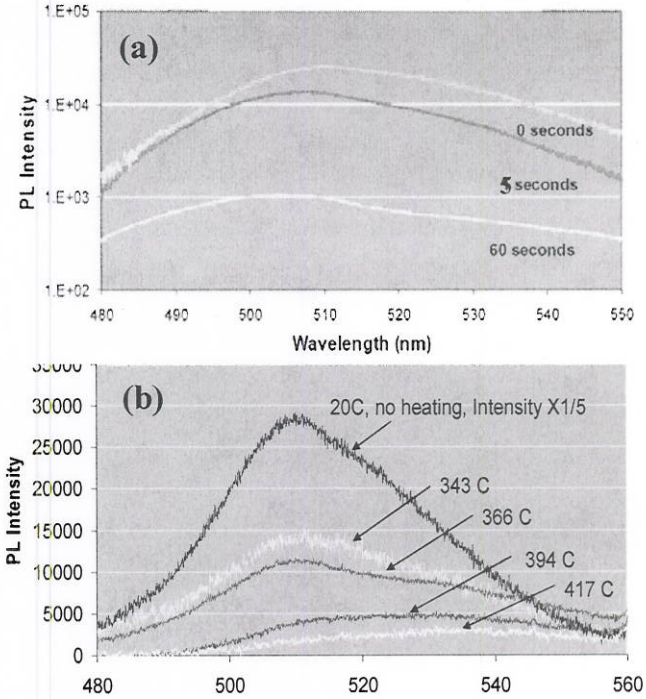

Figure 2.4.2 a) PL of QDs of 2nm in diameter after heated 5 and 60 seconds on a hotplate at the temperature of ~380 ^{0}C. b) Heated on Pt wire by 2 ms pulse current. All spectra were obtained under 200 fs blue excitation.

2.4.3 Wollaston Wire as Heater

Wollaston wire has wire size around a few microns. Lower power with fast heating pulse source can be used to simulate even fast heating and cooling events. Confined detection area in micron sized wire benefits the data acquisition repeatability. However, it has difficulties to deliver the QDs onto the wire due to fragility of thin wire and hydrophobicity by the surface forces as shown in Fig. 2.4.-3a. After QDs of 2 nm in size with PL emission peak around 520 nm (Fig. 2.4.-3b) were made the drop contact with the wire as shown in Fig. 2.4.-3a, the spectrum shape has been changed (Fig. 2.4.-3c). A red-shifted spectrum center might result from the weight of small dots decrease during drying process because of the larger size distribution in synthesizing smaller QDs resulting wider spectral broadening. Better deliver method and the wire surface treatment are required to carry out further experiment. On the other hand, this deliver method might be used to select or filter the size for colloidal QDs. Size control or uniformity of quantum dots, especially for small dots both in growth and selection are great challenges.

2.4.4 Ag particle coupled Quantum Dots

It has been shown that metal surface plasmon can enhance the dipole polarization. Our preliminary studies by simply mixing Ag particles size of 12 nm and 2 nm with QDs have shown no apparent enhancement or PL property changes under the both blue and green laser excitations. Surface treatment of both QDs and Ag particles and better mixing method, as well as plasmon resonant optical excitation might be required for further studies.

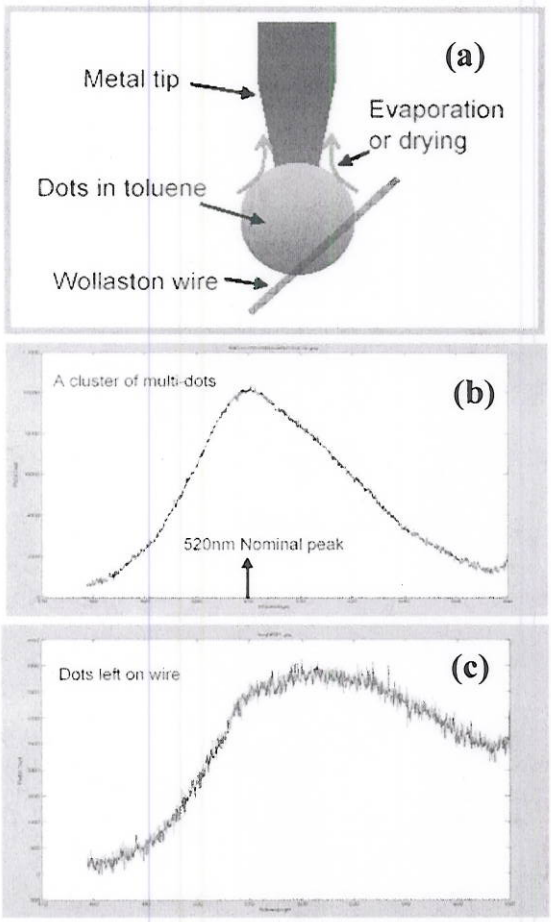

Figure 2.4.-3 a) Colloidal QDs delivery onto a Wollaston wire.(b) PL spectrum of 2nm sized QDs (c) PL spectrum from the wire after the delivery.

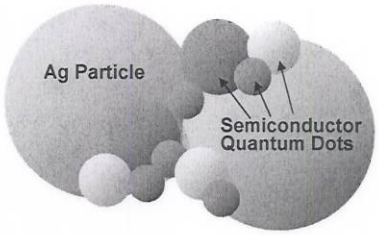

Figure 2.4-4 Complex sensors of Ag nanoparticles with QDs

3. Summary

We have demonstrated the feasibility of using Ag nanoparticles and quantum dots as temperature history sensors. We obtained quantitative relationship between heating temperature and Ag particle geometries and QDs PL properties. The relationships were used to fabricate and characterize thermal history sensors. Two kinds of thermal history sensors were invented. We showed that Ag nanoparticle size can record spatial distribution of temperature field created due to electron beam heating. For QDs, we showed that the particles are sensitive to ms heating. The experimental data have shown that we are on right track to achieve our goals.

Personal supported

At MIT: Dr. Xiaoyuan. Chen, research scientist, carried out photoluminescence experiment. Dr. Nitin Shukla also performed PL measurement and data analysis, and Kimberlee Collins contributed to optical system setup.

At BC: subcontract supported part of Mr. Hui Wang and part of Dr. Yucheng Lan.

Publications

1. Yucheng Lan, Hui Wang, Xiaoyuan Chen, Dezhi Wang, Gang Chen, and Zhifeng Ren, "Nanothermometer Using Single Crystal Silver Nanospheres", *Adv. Mater.* (2009) (Published Online: Aug 15 2009 11:17AM DOI: 10.1002/adma.200901313).

2. X. Chen, Y. Lan, L. Hu, Z. F. Ren and G. Chen, "Nanocrystals for Thermal History Sensor Application", *Sensors and Actuators A* (submitted).

Interactions/Transitions: None

Honors/Awards

G. Chen and Z. F. Ren, R&D 100 Award for High Performance Thermoelectric Materials, 2008.

G. Chen, ASME Heat Transfer Memorial Award, 2008.

G. Chen was named Carl Richard Soderberg Professor of Power Engineering at MIT, 2009.

G. Chen was elected to the US National Academy of Engineering, 2010.

DEPARTMENT OF DEFENSE

DEFENSE TECHNICAL
INFORMATION CENTER
8725 JOHN J. KINGMAN ROAD,
SUITE 0944
FT. BELVOIR, VA 22060-6201
ATTN: DTIC/OCA

DEPARTMENT OF DEFENSE CONTRACTORS

EXELIS, Inc.
1680 TEXAS STREET, SE
KIRTLAND AFB, NM 87117-5669
ATTN: DTRIAC